Hepatic p38γ exacerbates acetaminophen-induced acute liver injury via PI3K/Akt-dependent mechanisms

HUI FANG[1*], MIN SHU[2,3*], JIAJU WANG[4*], HENG TIAN[5*], JIANGUO ZHANG[5*], YING HU[6], HE LI[7], HUAN ZHOU[8], KANGSHENG GU[5] and ZHENHUA REN[1]

[1]Department of Human Anatomy, School of Basic Medical Sciences, Anhui Medical University, Hefei, Anhui 230032, P.R. China; [2]Inflammation and Immune Mediated Diseases Laboratory of Anhui Province, School of Pharmaceutical Sciences, Anhui Medical University, Hefei, Anhui 230032, P.R. China; [3]Anhui Key Lab of Bioactivity of Natural Products, Institute for Liver Diseases of Anhui Medical University, Anhui Medical University, Hefei, Anhui 230032, P.R. China; [4]Department of Oncology, Affiliated Drum Tower Hospital, Medical School of Nanjing University, Nanjing, Jiangsu 210008, P.R. China; [5]Department of Oncology, The First Affiliated Hospital of Anhui Medical University, Hefei, Anhui 230022, P.R. China; [6]State Key Laboratory of Pharmaceutical Biotechnology, School of Life Sciences, Nanjing University, Nanjing, Jiangsu 210023, P.R. China; [7]Emergency Department, The Second Affiliated Hospital of Anhui Medical University, Hefei, Anhui 230601, P.R. China; [8]Department of Clinical Trial Research Center, First Affiliated Hospital of Bengbu Medical University, Bengbu, Anhui 233004, P.R. China

Received July 9, 2025; Accepted February 10, 2026

DOI: 10.3892/ijmm.2026.5855

Abstract. An acetaminophen (APAP) overdose can result in acute and chronic liver injury. Thus, the discovery of biomarkers for the management of APAP-induced liver injury is crucial from a therapeutic standpoint. As one of the four isoforms of p38 mitogen activated protein kinases, p38γ plays a notable role in the inflammatory processes associated with various diseases. However, the underlying molecular mechanisms of p38γ in liver injury are largely unknown. In the present study, it was demonstrated that AML-12 cells and liver tissues induced with APAP had elevated p38γ expression. DCFH-DA fluorescent probe and oil red O staining was used to investigate oxidative stress and lipid metabolism in APAP-induced AML-12 cells and western blotting was used to assess the expression levels of oxidative stress and lipid metabolism-related protein inflammatory cytokines. The results showed that p38γ knockdown significantly attenuated the inflammatory response, oxidative stress and lipid accumulation, whereas overexpression of p38γ exhibited the opposite effect. Downstream, p38γ induced the activation of the PI3K/Akt signaling pathway via upregulation of phosphorylated (p-)PI3K and p-Akt levels. Additionally, TargetScan analysis and dual luciferase reporter assays showed that microRNA-125 selectively targeted the 3'-untranslated region of p38γ, resulting in the repression of APAP-induced inflammation, lipid accumulation and oxidative stress. Furthermore, adeno-associated virus 9-short hairpin RNA p38γ was used via tail vein injection to cause p38γ downregulation *in vivo*. The results showed that knockdown of p38γ significantly reduced the inflammatory response, lipid accumulation and oxidative stress in APAP-induced liver injury. Together, these findings demonstrated that targeting p38γ could be an effective approach for treating liver injury caused by APAP.

Introduction

The liver functions as a detoxifying organ once foreign substances enter the human body, while excessive microbial byproducts can induce damage to the liver (1). Acetaminophen (APAP) is one of the most widely used analgesics and antipyretic drugs worldwide (2,3). However, overdose of APAP is the leading cause of drug-induced liver injury (DILI) and liver failure in several countries, accounting for ~400,000 deaths every year in China alone (3-5). Overdose of APAP results in the depletion of glutathione (GSH), leading to the covalent binding of excess *N*-acetyl-p-benzoquinone imine (NAPQI) to mitochondrial proteins. This triggers oxidative stress, mitochondrial dysfunction and ultimately hepatocyte necrosis (6-10). At present, *N*-acetylcysteine (NAC) is the standard clinical antidote for the treatment of APAP poisoning and its primary role is to replenish hepatic GSH; however, the timeframe of administration and gastrointestinal side-effects of NAC have limited its clinical use (11,12). Consequently, there

Correspondence to: Professor Zhenhua Ren, Department of Human Anatomy, School of Basic Medical Sciences, Anhui Medical University, 81 Meishan Road, Shushan, Hefei, Anhui 230032, P.R. China
E-mail: renzhenhua1975@163.com

Professor Kangsheng Gu, Department of Oncology, The First Affiliated Hospital of Anhui Medical University, 218 Jixi Road, Shushan, Hefei, Anhui 230022, P.R. China
E-mail: gukangsheng@ahmu.edu.cn

*Contributed equally

Key words: acetaminophen, p38γ, microRNA-125, liver injury, inflammation

is a pressing need for biomarkers that exhibit both specificity and sensitivity in predicting the development or resolution of acute liver injury. Such biomarkers could prove instrumental in mitigating APAP-induced liver injury and reducing associated mortality rates.

There are four main isoforms of the p38 mitogen-activated protein kinase (MAPK) family: p38α, p38β, p38γ and p38δ. These isoforms may be categorized into two groups: One comprising p38α/β and the other including p38γ/δ (13). Although the p38 isoforms are similar in sequence and share common upstream kinases, they may have unrelated or even antagonistic roles in development and disease (14-16). Notably, p38γ (also known as MAPK12, ERK6 or SAPK3) can be activated by stress and mitogenic signals (17). p38γ is expressed predominantly in muscle tissue, where it promotes myoblast differentiation into myotubes. p38γ mRNA is upregulated in several types of cancer, such as colon cancer (18-20). A study has shown that p38γ exhibits substrate selectivity and inhibition sensitivity similar to those of traditional cyclin-dependent kinase (CDKs), hence functioning as a CDK-like kinase (21). Notably, retinoblastoma (Rb), a well-known protein linked to tumor suppression, may be phosphorylated by p38γ, which activates essential cyclins (E1/A). This, in turn, facilitates cancer cell growth and proliferation, including hepatocellular carcinoma (HCC) and other types of cancer (22). Additionally, several findings indicate that p38γ may link inflammation to tumorigenesis (23,24). For example, Yin *et al* (25) demonstrated that p38γ was activated by inflammation in the mouse colon and knockdown of p38γ attenuated the inflammatory response, decreased proinflammatory cytokine expression and inhibited inflammation-associated colon tumorigenesis. Furthermore, biopsies of human HCC showed high expression of p38γ (22). Additionally, targeting p38γ has been shown to synergistically enhance sorafenib-induced cytotoxicity in HCC (26), further supporting its functional significance in liver pathobiology. Moreover, p38γ expression is significantly elevated in the livers of patients, diagnosed with non-alcoholic fatty liver disease (NAFLD). Notably, our previous study showed a direct link between p38γ and the pathogenesis of liver injury (27). It was shown that p38γ expression is upregulated in the liver after exposure to APAP and ethanol. Inhibition of p38γ attenuated ethanol- and APAP-induced AML-12 cell injury. Moreover, the knockdown of p38γ repressed the inflammation, lipid accumulation and oxidative stress in ethanol- and APAP-induced liver injury. Furthermore, previous studies have indicated that mice that lack p38γ exhibit resistance to diet-induced fatty liver, as well as improved glucose tolerance and reduced hepatic triglyceride accumulation (27,28). It has been previously shown that p38γ kinases regulate inflammation by influencing macrophage production of tumor necrosis factor (TNF)-α (29,30) and T-cell activation (31). These findings provide a strong rationale for investigating the specific role and mechanism of p38γ in APAP hepatotoxicity. In summary, it is highly plausible that p38γ may exert a significant influence on inflammation and oxidative stress in the context of APAP-mediated liver injury.

MicroRNAs (miRNAs) are short non-coding RNAs, typically 20-22 nucleotides in length, that regulate gene expression by binding to the 3'-untranslated region (UTR) of target mRNAs (32,33). The dysregulation of miRNAs is associated with hepatic metabolic disorders, injury, fibrosis and tumorigenesis (34-37). For example, Ren *et al* (38) reported that aging exacerbates alcohol-induced liver injury in mice and humans through suppression of the sirtuin 1-C/EBPα/miR-223 axis, highlighting the significance of miRNAs in liver disease. Therefore, the present study explored the upstream regulatory factors of p38γ using bioinformatics analysis.

The present study aimed to investigate functional role of p38γ in APAP-induced liver injury and clarify its upstream regulatory mechanisms. AML-12 cells and C57BL/6J mice were used to establish a liver injury model induced by APAP. Multiple experimental approaches were utilized, including RNA-sequencing (RNA-seq) to analyze gene expression profiles, western blotting and reverse transcription-quantitative PCR (RT-qPCR) to detect the expression of target molecules, luciferase reporter assays to verify miRNA-mRNA binding interactions and biochemical analyses to assess oxidative stress and lipid metabolism indicators. In addition, adeno-associated virus 9 (AAV9)-mediated short hairpin RNA (shRNA) was used for *in vivo* p38γ knockdown. In conclusion, these strategies elucidated the role of p38γ and the regulatory effect of miR-125 in APAP-induced liver injury, offering novel insights into potential therapeutic targets.

Materials and methods

Reagents. The AML-12 cells (cat. no. CL-0602) were provided by Wuhan Pricella Biotechnology Co., Ltd. (Elabscience Bionovation Inc.). Assay kits for alanine aminotransferase (ALT; cat. no. C009-2-1), aspartate aminotransferase (AST; cat. no. C010-2-1), GSH (cat. no. A006-2-1), malondialdehyde (MDA; cat. no. A003-1-2) and superoxide dismutase (SOD; cat. no. A001-3-2) were obtained from Nanjing Jiancheng Institute of Bioengineering. The anti-p38γ (cat. no. 20184-1-AP), anti-IL-6 (cat. no. 21865-1-AP), anti-IL-1β (cat. no. 16806-1-AP), anti-albumin (cat. no. 16475-1-AP), Akt (cat. no. 10176-2-AP), anti-phosphorylated (p-)Akt (cat. no. 66444-1-Ig), anti-TNF-α (cat. no. 17590-1-AP), anti-peroxisome proliferator-activated receptor (PPAR)-α (cat. no. 66826-1-Ig), anti-sterol regulatory element-binding protein (SREBP)-1 (cat. no. 14088-1-AP) and anti-Fasn (cat. no. 10624-2-AP) antibodies were purchased from Proteintech Group, Inc. Anti-NADPH oxidase 4 (NOX4) (cat. no. A11274) and anti-inducible nitric oxide synthase (iNOS) (cat. no. A14031) were purchased from ABclonal Biotech Co., Ltd. Anti-β-actin (cat. no. AF7018), anti-PI3K (cat. no. AF3241) and anti-p-PI3K (cat. no. AF6241) were purchased from Affinity Biosciences, Ltd. ELISA kits for IL-1β (cat. no. MLB00C-1), IL-6 (cat. no. M6000B-1) and TNF-α (cat. no. MTA00B-1) were purchased R&D Systems, Inc. The detection of IL-1β, IL-6 and TNF-α was carried out in accordance with the manufacturer's instructions.

Animal experiments. All animal care and experimental protocols were approved by the Anhui Medical University Experimental Animal Ethics Committee (approval no. LLSC20241364). The protocols for the use and care of medical laboratory animals were followed in all operations. For the animal experiments, 8-week-old male C57BL/6J mice weighing 20-22 g were obtained from Jiangsu GemPharmatech Co., Ltd. Mice were kept in a specific pathogen-free facility at

the Anhui Medical University Experimental Animal Center. The number of animals used in each group was 6, with a total of 24 C57BL/6J mice used in the experiment. All 24 mice were euthanized at the scheduled time point and no mice were found dead during the experiment. The housing conditions were set as follows: The breeding room temperature was maintained at 22±2˚C, the relative humidity was 50±10% and the light/dark cycle was 12/12 h. Mice had free access to standard laboratory chow and sterile drinking water throughout the experiment.

Before the animal model was established, mice were allowed to acclimatize for 1 week, during which they were fed an adaptable diet and had access to sufficient quantities of water. Following randomization, the animals were weighed and split into four groups: Normal, APAP, APAP + AAV9-Empty and APAP + AAV9-shRNA-p38γ. For the intervention groups, mice were slowly injected via the tail vein with either AAV9-Empty or AAV9-shRNA-p38γ. The AAV9-shRNA-p38γ used in the present study was provided by Hanbio Biotechnology Co., Ltd. The sequences were as follows: 5'-GGCCAAGAACUACAUGGAATT-3' and 5'-UUCCAUGUAGUUCUUGGCCTT-3'. An intraperitoneal dose of APAP (250 mg/kg; Beijing Solarbio Science & Technology Co., Ltd.) was used to induce liver injury (39,40) 14 days after the AAV injection. Liver injury was induced in the APAP, APAP + AAV9-Empty and APAP + AAV9-shRNA-p38γ groups via an intraperitoneal injection of APAP. At 24 h after APAP injection, blood was collected via retro-orbital bleeding using sterile heparinized microhematocrit capillary tubes in the SPF animal room. Mice were anesthetized with isoflurane inhalation (induction 3-4%, maintenance 1.5-2%) prior to collection. In total, 0.5-1.0 ml of blood was obtained from each mouse and transferred into plain serum separation tubes. The samples were allowed to clot at room temperature for 30 min, and serum was separated by centrifugation at 2,000 x g for 10 min at 4˚C. Serum was stored at -80˚C until analysis. The mice were euthanized 24 h after APAP administration using CO_2 at 30-70% vol/min displacement in compliance with the AVMA guidelines: 2020 Edition (41). The absence of a heartbeat and respiratory movement, along with a lack of response to physical stimulation, were used to confirm animal death. The health and behavior of the mice were monitored twice a day during the acclimatization and experimental periods, including the observation of mental state, activity, food intake, water intake and hair condition. The humane endpoints followed in the present study included: Severe weight loss (>20% of the body weight), inability to eat or drink independently, severe lethargy, abnormal posture, difficulty in breathing and severe liver injury-related symptoms. No animals reached these humane endpoints during the experiment and all mice were euthanized as scheduled.

The livers were collected and divided into tiny pieces, then fixed in 4% paraformaldehyde at room temperature for 48 h for histology. The remainder of the tissue was frozen in liquid nitrogen and kept at -80˚C for further examination. To minimize bias, group assignment was performed randomly using a computer-generated random number sequence. Furthermore, while the investigators administering the treatments were necessarily aware of group identities, all subsequent data acquisition and analysis were performed under blinded conditions. The personnel conducting histopathological scoring, biochemical assays, western blot quantification and statistical analysis were unaware of the group codes until after all data collection was complete.

Cell culture. The AML-12 cells were cultured in DMEM/F-12 media (Gibco; Thermo Fisher Scientific, Inc.; cat. no. 11320033) supplemented with 10% fetal bovine serum (Gibco; Thermo Fisher Scientific, Inc.; cat. no. 10099141), 1% penicillin-streptomycin solution (10,000 units/ml penicillin and 10,000 μg/ml streptomycin; Gibco; Thermo Fisher Scientific, Inc.). The cells were maintained in a 37˚C incubator with 5% CO_2. Cells were treated with 10 mM APAP for 24 h to establish an *in vitro* model of liver injury (42,43). Cells between passages 5 and 15 were used for all experiments. For treatment, cells were seeded and allowed to reach 70-80% confluency before the addition of APAP or transfection.

Immunohistochemistry (IHC). For IHC, 4 μm sections were cut from the paraffin-fixed liver tissues. Following deparaffinization and rehydration, heat-induced epitope retrieval was performed by incubating the slides in sodium citrate buffer (10 mM, pH 6.0) at 95˚C for 20 min. The sections were then allowed to cool to room temperature. After washing with PBS, the sections were incubated with 3% hydrogen peroxide for 10 min at room temperature to quench endogenous peroxidase activity, washed three times with PBS for 5 min each, then blocked with 2% BSA (Sigma-Aldrich; Merck KGaA; cat. no. A8806) for 30 min at room temperature. Subsequently, after overnight incubation at 4˚C with anti-TNF-α, anti-IL-1β or anti-IL-6 (all 1:150), the sections were washed three times with PBS for 5 min each and then incubated for 1 h at room temperature with a biotinylated IgG secondary antibody (Proteintech Group, Inc.; cat. no. 16795-1-AP; 1:200). Next, the sections were washed with PBS, then incubated with Vectastain ABC reagent for 1 h at room temperature and diaminobenzidine (Shanghai Aladdin Biochemical Technology Co., Ltd.) substrate solution for 5 min at room temperature. Finally, the slides were counterstained with hematoxylin at room temperature for 3 min and examined under a light microscope.

Immunofluorescence. The procedure for immunofluorescence microscopy was performed as described previously (33,44). Briefly, cells were plated on coverslips coated with 10 μg/ml fibronectin. After fixing the cells for 10 min at room temperature with 3.7% paraformaldehyde, the cells were washed three times with PBS. Cells were permeabilized with 0.5% Triton X-100 at 37˚C for 5 min. Subsequently, the cells were blocked with goat serum (Beyotime Biotechnology; cat. no. C0265) at room temperature for 30 min, then incubated with anti-p38γ and anti-albumin primary antibodies (both 1:100) in a wet chamber at 4˚C overnight. This was followed by incubation with Alexa Fluor 488-conjugated anti-rabbit/mouse (cat. no. P11047; 1:500; Invitrogen; Thermo Fisher Scientific, Inc.) or Alexa Fluor 594-conjugated anti-rabbit (cat. no. S32356; 1:500; Invitrogen; Thermo Fisher Scientific, Inc.) secondary antibodies for 1 h at 37˚C. Cells were washed with PBS, then cell nuclei were counterstained with DAPI (1 μg/ml; Beyotime Biotechnology) for 5 min at room temperature. The cells were mounted with Prolong Gold anti-fade reagent and imaged using a YB710FL fluorescence microscope.

Western blotting. The radioimmunoprecipitation assay lysis buffer (Beyotime Biotechnology; cat. no. P0013B) supplemented with 1 mM phenylmethanesulfonyl fluoride was used to extract total protein from the liver tissues and cultured cells, then protein concentration was measured using a BCA protein assay kit (Beyotime Biotechnology). Equal quantities of protein (30 μg) were loaded per lane on a 10% SDS gel, resolved using SDS-PAGE, transferred to PVDF membranes at 400 V for 30 min and then blocked for 2 h at room temperature in 5% non-fat milk in Tris-buffered saline with 0.05% Tween-20 (TBST). Subsequently, the membranes were incubated with primary antibodies at 4˚C overnight. The following day, the membranes were washed TBST and incubated with horseradish peroxidase-conjugated secondary antibodies (cat. no. 7074S; Cell Signaling Technology, Inc.) diluted in blocking buffer (1:5,000) for 1 h at room temperature. An enhanced chemiluminescence kit (SuperSignal west pico trial kit; Pierce; Thermo Fisher Scientific, Inc.) was used to visualize signals. The signals were captured using a ChemiDoc MP Imaging System (Bio-Rad Laboratories, Inc.). β-actin was used as the loading control. Densitometry analysis was performed using ImageJ software (version 1.53k; National Institutes of Health). The primary antibodies were diluted as follows: Anti-PI3K (1:1,000), anti-p-PI3K (1:1,000), anti-Akt (1:1,000), anti-p-Akt (1:1,000), anti-p38γ (1:1,000), anti-IL-6 (1:1,000), anti-IL-1β (1:2,000) anti-TNF-α (1:1,000), anti-NOX4 (1:2,000), anti-iNOS (1:2,000), anti-PPAR-α (1:1,000), anti-SREBP-1 (1:1,000), anti-Fasn (1:1,000) and anti-β-actin (1:1,000).

Luciferase reporter assay. The putative wild-type (WT) or mutant (MUT) 3'-UTR of p38γ containing the miR-125 binding site was synthesized and cloned into the pmirGLO Dual-Luciferase vector (Promega Corporation; cat. no. E1330). AML-12 cells were co-transfected with the constructed reporter vectors (luc-p38γ-WT or luc-p38γ-MUT) and either miR-125 mimics or negative control (NC) mimics using Lipofectamine™ 3000 (Invitrogen; Thermo Fisher Scientific, Inc.). After 48 h, luciferase activity was measured using the Dual-luciferase Reporter Assay Kit (Promega Corporation) according to the manufacturer's protocol. Firefly luciferase activity was normalized to *Renilla* luciferase activity for each sample.

Biochemical analyses. The levels of serum (0.5-1.0 ml per mouse) from mice ALT, AST, MDA, GSH and SOD were measured using commercial kits according to the manufacturer's instructions.

Histological examination. Liver specimens were fixed in 4% paraformaldehyde, embedded in paraffin and cut into 50 μm-thick sections. Samples were stained with hematoxylin and eosin (H&E) as follows: Initially, samples were incubated with hematoxylin for 5 min and then washed with water, differentiated with hydrochloric acid solution for ~3 sec, washed with tap water, counterstained with ammonia solution for ~3 sec and washed with tap water again. Under the microscope, nuclei appeared pale blue to blue, with a pale blue or nearly colorless background. Sections were dehydrated sequentially in 85 and 95% ethanol solutions for 4 min each, then immersed in eosin solution for 1-2 min. Dehydration was performed using absolute ethanol, followed by clearing with n-butanol and xylene. Sections were then transferred to a square container containing clean xylene and mounted with neutral resin.

For the Masson's trichrome staining procedure, paraffin-embedded sections were dewaxed, immersed in water for 2 min, then sequentially immersed in xylene, absolute ethanol, 95% ethanol, 80% ethanol and 70% ethanol for varying durations, followed by washing with distilled water. Sections were then immersed in ferric hematoxylin stain for 3-8 min, then washed under running water. Subsequently, sections were stained with Alizarin Red-Acid Fuchsin for 10 min. Next, the sections were placed in phosphomolybdic acid for differentiation for several seconds, then washed with water, followed by staining in aniline blue solution for 5 min and washing with 0.2% glacial acetic acid. Sections were sequentially immersed in 95% ethanol, anhydrous ethanol and xylene for varying durations. After removing sections from xylene, they were air-dried briefly and mounted in neutral resin. Sirius red staining for collagen was performed according to the manufacturer's protocol (Beyotime Biotechnology; cat. no. C1006).

All stained sections were examined under a light microscope (Nikon Eclipse Ci-L) by two independent pathologists blinded to the experimental grouping. All steps were performed at room temperature.

Detection of intracellular reactive oxygen species (ROS). To determine the intracellular ROS levels, a fluorescence-based probe sensitive to oxidation, 2',7'-dichlorodihydrofluorescein diacetate (DCFH-DA; Beyotime Biotechnology) was used. After treatment, cells were washed twice with PBS and then incubated for 20 min at 37˚C with 10 μmol/l DCFH-DA. Non-specific esterase within the cells deacetylate DCFH-DA and ROS are then oxidized to produce the fluorescent chemical 2',7'-dichlorofluorescein (DCF). The cells were then washed three times with pure DMEM. Fluorescence microscopy (Yuescope; cat. no. YB710FL) was used to detect the ROS levels with excitation/emission settings of 485/535 nm. To validate the assay, untreated cells were used to establish the baseline fluorescence (negative control) and cells treated with hydrogen peroxide (200 μM for 30 min) were used as a positive control to confirm the responsiveness of the DCFH-DA probe.

RT-qPCR. Total RNA was extracted from tissues or cells using TRIzol® reagent (Invitrogen; Thermo Fisher Scientific, Inc.; cat. no. 15596026) according to the manufacturer's protocol. RNA concentration and purity were assessed using a NanoDrop™ spectrophotometer (Thermo Fisher Scientific, Inc.). A total of 1 μg total RNA was reverse-transcribed into cDNA using the Transcriptor First-Strand cDNA Synthesis Kit (Roche Diagnostics GmbH; cat. No 04379012001) with oligo(dT) primers according to the manufacturer's protocol. qPCR was performed using FastStart Universal SYBR Green Master (Rox) (Roche Diagnostics GmbH; cat. no. 04913850001) on a QuantStudio 3 Real-Time PCR System (Applied Biosystems, Thermo Fisher Scientific, Inc.). The thermocycling conditions were as follows: 95˚C for 30 min, followed by 40 cycles of 95˚C for 15 sec and 60˚C for 30 min. All reactions were run in triplicate. The relative mRNA expression levels were calculated

using the $2^{-\Delta\Delta Cq}$ method (45) and normalized to GAPDH. The sequences of the primers are listed in Table I.

Cell transfection. To downregulate or upregulate the expression of miR-125 and p38γ, miR-125 mimic, miR-125 inhibitor, p38γ small interfering (si)-RNA, p38γ plasmid (pEGFP-C1-p38γ) or corresponding control constructs were used. A total of 50 nM nucleic acid constructs (miR-125 mimic, miR-125 inhibitor or p38γ siRNA) and 2 μg plasmid DNA (pEGFP-C1-p38γ) or corresponding control constructs were transfected using Lipofectamine™ 3000 (Invitrogen; Thermo Fisher Scientific, Inc.) according to the manufacturer's protocol. Cells were transfected for 6 h, after which, the culture medium was changed and APAP was added. AML-12 cells were cultured at 37˚C in a humidified incubator supplied with 5% CO_2 for 24 h and then collected for RT-qPCR or western blot analysis. All transfected constructs were purchased from Shanghai GenePharma, Co., Ltd. The sequences of the miR-125 mimic, miR-125 inhibitor, p38γ-siRNA and the corresponding NCs are listed in Table II.

ELISA. The supernatants of AML-12 cells in the different treatment groups were collected and the expression levels of TNF-α, IL-1β and IL-6 were assessed by ELISA kits according to the manufacturer's instructions.

MTT. MTT reagent was purchased from Sigma-Aldrich (Merck KGaA). Before the experiment, MTT reagent was prepared into a 5 mg/ml working solution with serum-free medium, filtered and sterilized, and stored at 4˚C in the dark for later use. AML-12 cells in the logarithmic growth phase were seeded into 96-well culture plates at a density of $1x10^4$ cells per well with a volume of 100 μl per well and cultured in a 37˚C, 5% CO_2 incubator until the cells adhered to the wall. Then, different concentrations of APAP treatment solution were added (the control group was added with the same volume of solvent) and cultured for 0, 6, 12, 24 and 48 h respectively. After the incubation, 20 μl of MTT working solution was added to each well and the incubation was continued for 4 h to form purple formazan crystals. After the incubation, the supernatant in the wells was carefully aspirated and discarded, 150 μl of DMSO was added to each well and the mixture was shaken at low speed on a shaker for 10 min to ensure complete dissolution of formazan crystals. A microplate reader was used to measure the absorbance of each well at a wavelength of 570 nm with a reference wavelength of 630 nm. The cell viability of the control group was set as 100% and the relative cell viability of each treatment group was calculated. Each treatment group was set with 3 replicate wells and the experiment was independently repeated 3 times.

Isolation and culture of primary hepatocytes. The male C57BL/6J mice (8 weeks old, body weight 20-22 g) were obtained from Jiangsu GemPharmatech Co., Ltd. Mice were housed under specific pathogen-free conditions at 22±2˚C, 50±10% relative humidity and a 12 h light/dark cycle, with free access to standard chow and water. Before the hepatocytes were isolated, mice were allowed to acclimatize for 1 week. Then, isoflurane (induction 3-4%, maintenance 1.5-2%) was used to anesthetize the mice, followed by perfusion with a washing buffer [Hank's balanced salt solution (HBSS; Beyotime Biotechnology; cat. no. C0218) with 0.1% EDTA (Sigma-Aldrich; Merck KGaA; cat. no. E6758)] via the inferior vena cava. Next, a digestive solution (HBSS with 0.5 mg/ml collagenase D; Roche Diagnostics GmbH; cat. no. 11088866001) was used for perfusion. Once the perfusion was complete, the mice were euthanized using CO_2 and the livers were extracted and primary hepatocytes were isolated by carefully slicing the liver lobes. The cells underwent filtration, centrifugation at 50 x g for 5 min at 4˚C, washing twice with cold William's E medium (Gibco; Thermo Fisher Scientific, Inc.; cat. no. A1217601) by centrifugation at 50 x g for 5 min at 4˚C, and were resuspended in William's E medium. They were then seeded at a suitable density for further experiments.

Table I. Primer sequences for reverse transcription-quantitative PCR.

Gene	Sequence (5'-3')
p38γ	Forward: GAGAGTTGCGCCTCCTCAAA
	Reverse: CACTCAGGGTCTCATGCTTCA
TNF-α	Forward: AGGCACTCCCCCAAAAGATG
	Reverse: CCACTTGGTGGTTTGTGAGTG
IL-6	Forward: CTGCAAGAGACTTCCATCCAG
	Reverse: AGTGGTATAGACAGGTCTGTTGG
IL-1β	Forward: TGGATGCTCTCATCAGGACAG
	Reverse: GAAATGCCACCTTTTGACAGTG
U6	Forward: CTCGCTTCGGCAGCACATATACT
	Reverse: ACGCTTCACGAATTTGCGTGTC
miR-125	Forward: GCUCCCUGAGACCCUAAC
	Reverse: CAGTGCAGGGTCCGAGGT
GAPDH	Forward:GTCGATGGCTAGTCGTAGCATCGAT
	Reverse: TGCTAGCTGGCATGCCCGATCGATC

miR-125, microRNA-125.

RNA-seq analysis. Total RNA was extracted from AML-12 cells, both untreated and treated with 10 mM APAP, using TRIzol reagent, with three replicates per group. NanoDrop spectrophotometry was used to evaluate the concentrations, quality and integrity of the extracted RNA. Afterward, 3 μg of RNA (RNA integrity number, 10.0; a score of 10.0 indicates intact, high-quality RNA with no degradation) was extracted from each sample, which was sequenced and analyzed by Shanghai Personal Biotechnology Co., Ltd. Briefly, the construction of the sequencing library was completed using the TruSeq RNA Sample Preparation Kit (cat. no. RS-122-2001; Illumina, Inc.). Library quantification was achieved through a two-step method: Preliminary quantification was performed using RT-qPCR, followed by precise detection using the Agilent High Sensitivity DNA Kit on the Agilent 2100 Bioanalyzer System (Agilent Technologies, Inc.). After quantification, the library was sequenced on the Illumina Novaseq 6000 sequencing platform (300 cycles; cat. no. 20012860; Illumina, Inc.), generating paired-end reads of 150 bp in length. The final library was loaded at a concentration

Table II. Sequences of miR-125 mimics, miR-125 inhibitor, p38γ-siRNA and the corresponding NCs.

Gene	Sequence (5'-3')
p38γ-siRNA	Sense: GGCCAAGAACUACAUGGAATT
	Anti-sense: UUCCAUGUAGUUCUUGGCCTT
siRNA NC	Sense: UUCUCCGAACGUGUCAGGUTT
	Anti-sense: ACGUGACACGUUCGGAGAATT
Mimic NC	Sense: ACACGUCAGCAUUAACUCCUUG
	Anti-sense: UGUGCAGUCGUAAUUGAGGAAC
miR-125 mimic	Sense: UCCCUGAGACCCUUUAACCUGUGA
	Anti-sense: ACAGGUUAAAGGGUCUCAGGGAUU
Inhibitor NC	CAGUACUUUUGUGUAGUACAA
miR-125 inhibitor	UCACAGGUUAAAGGGUCUCAGGGA

siRNA, small interfering RNA; miR-125, microRNA-125; NC, negative control.

of 150 pM, determined by RT-qPCR and verified using the Agilent 2100 Bioanalyzer with the High Sensitivity DNA Kit. The raw sequencing data was filtered using FastQC software (version 0.11.9; https://www.bioinformatics.babraham.ac.uk/projects/fastqc/) to remove low-quality sequences and then the qualified reads were aligned to the human reference genome (version hg38) using HISAT2 alignment software (version 2.2.1; https://daehwankimlab.github.io/hisat2/). HTSeq v0.9.1 (https://htseq.readthedocs.io/en/release_0.9.1/) was used to calculate read counts, which were then normalized and expressed as fragments per kilobase of transcript per million mapped reads. Genes showing a fold change >2 and a normalized P<0.05 were considered differentially expressed. A heatmap of differentially expressed genes (DEGs) was created using R (version 4.2.2; https://www.R-project.org/). Gene Ontology (GO) (http://www.geneontology.org/) was employed to analyze biological processes and the Kyoto Encyclopedia of Genes and Genomes (KEGG) was used for pathway analysis. Unlike the previous analyses that focused on identifying DEGs by filtering with fold change >2 and normalized P<0.05, and visualizing DEGs via a heatmap, GO_BP enrichment, KEGG analysis and Gene Set Enrichment Analysis were performed on DEGs specifically to annotate their biological functions, enrich associated biological processes and explore the involved signaling pathways. Circle plots were used to illustrate the DEGs associated with specific BP terms.

Statistical analysis. Data are presented as the mean ± SD of three repeats. One-way ANOVA with Bonferroni correction was used to compare multiple groups. Otherwise, a two-tailed unpaired t-test was used. All data were analyzed using SPSS (version 21.0; IBM Corp.). P<0.05 was considered to indicate a statistically significant difference.

Results

p38γ expression is increased in APAP-induced liver injury. To assess p38γ expression during the progression of liver injury, a liver injury model was established using APAP. H&E staining was used to determine the degree of liver injury (Fig. 1A). Additional analysis showed that ALT and AST activity was increased compared with the normal group (Fig. 1B). IHC analysis showed markedly increased levels of TNF-α, IL-6 and IL-1β (Fig. 1A). These results were further confirmed by western blot analysis (Fig. 1C). Further western blot analysis showed a significant decrease in the expression level of PPAR-α, whereas the SREBP-1, Fasn, iNOS and NOX4 expression levels were increased compared with the normal group (Fig. 1D and E). Next, APAP was used to construct a liver injury cell model *in vitro*. To explore the pharmacological effects of APAP, an MTT assay was conducted after 0, 6, 12, 24 and 48 h of incubation. The results showed that a reduction in cell viability from 99.33 to 51.67% was observed after incubating with APAP for 24 h (Fig. S1A). In addition, the expression of IL-6 and p38γ in AML-12 cells treated with APAP increased and peaked after 24 h of treatment (Fig. S1B). A liver injury model in AML-12 cells was established using APAP at 0, 2.5, 5, 10 and 20 mM. As shown in Fig. S1C, a reduction in cell viability from 99.67 to 52.00% was observed after incubating with 10 mM of APAP for 24 h. Additionally, the western blot results showed that APAP significantly increased the p38γ and p-Akt expression levels compared with the normal group, which peaked with APAP treatment at 10 mM (24 h) (Fig. S1D). Hence, AML-12 cells were treated with APAP at 10 mM for 24 h. The results showed that the expression levels of TNF-α, IL-6, IL-1β, SREBP-1, Fasn, iNOS and NOX4 was increased in AML-12 cells treated with APAP compared with the normal group (Fig. 1F-H).

Next, RNA-seq analysis was used to compare gene expression in control AML-12 cells and APAP-induced AML-12 cells. A total of 2,138 significantly DEGs were identified, consisting of 766 upregulated and 1,372 downregulated genes. Our previous study indicated that p38γ was upregulated in the liver injury after exposure to APAP and ethanol, and its inhibition could alleviate the cell damage and inflammatory response in the combined model (27). Moreover, another of our studies demonstrated that p38γ significantly increased during the NAFLD process and knockdown of p38γ could inhibit lipid accumulation in liver cells by suppressing the activation of the JAK/STAT signaling pathway (28), providing an important preliminary foundation for the present study. Additionally, p38γ is increasingly recognized as being related

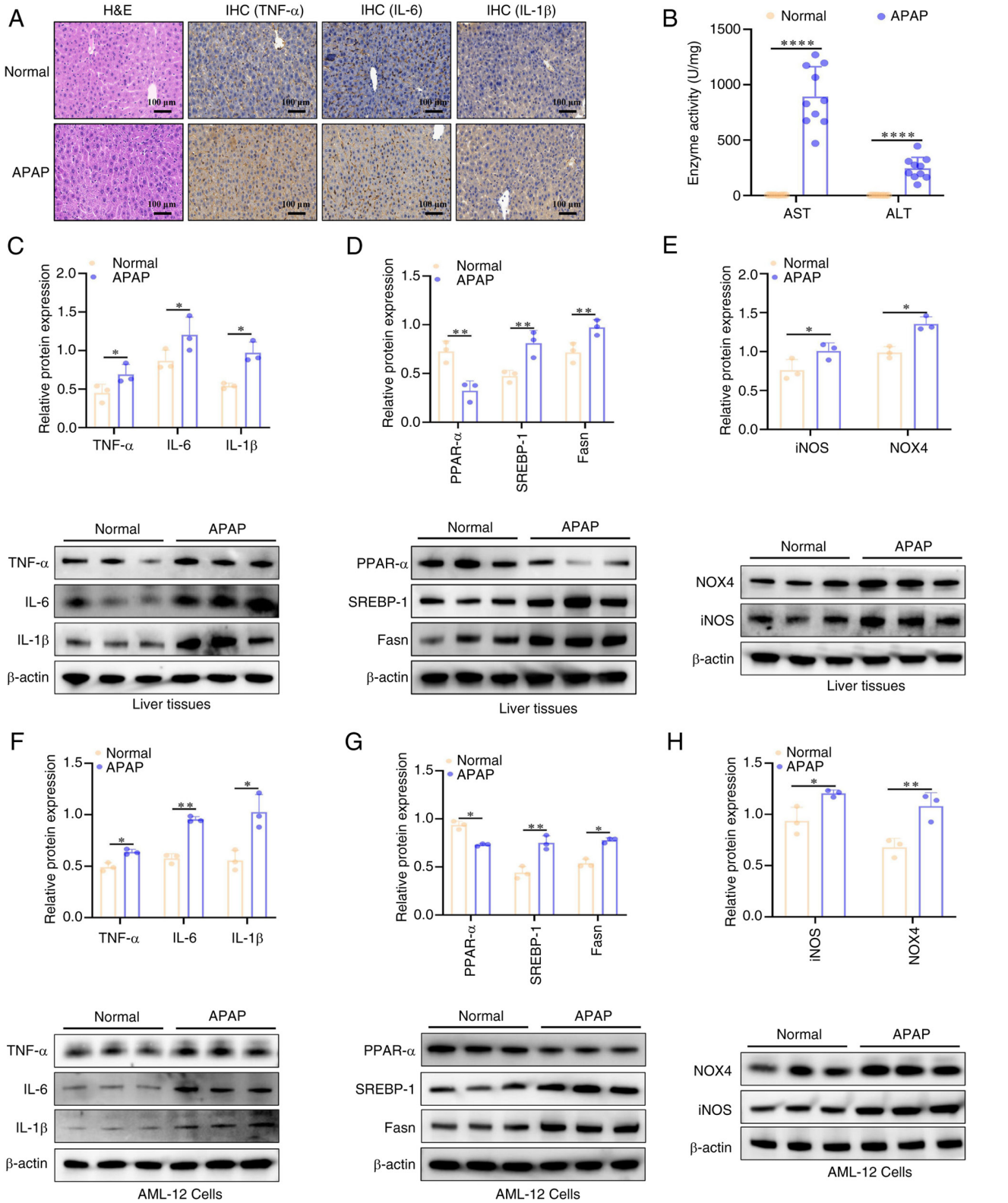

Figure 1. Establishment of the APAP-induced liver injury in mice and cell models. (A) Paraffin-embedded liver sections underwent H&E staining as well as TNF-α, IL-6 and IL-1β immunostaining; scale bars, 100 μm. (B) Serum ALT and AST levels were measured in APAP-induced mice (n=6). (C) Representative western blots and densitometry analysis of TNF-α, IL-6 and IL-1β expression in liver extracts prepared from APAP-induced mouse liver tissues. (D) Representative western blots and densitometry analysis of SREBP-1, PPAR-α and Fasn expression in liver extracts prepared from APAP-induced mouse liver tissues. (E) Representative western blots and densitometry analysis of iNOS and NOX4 expression in liver extracts prepared from APAP-induced mouse liver tissues. (F) Representative western blots and densitometry analysis of TNF-α, IL-6 and IL-1β expression in APAP-induced AML-12 cells. (G) Representative western blots and densitometry analysis of SREBP-1, PPAR-α and Fasn expression in APAP-induced AML-12 cells. (H) Representative western blots and densitometry analysis of iNOS and NOX4 expression in APAP-induced AML-12 cells. Data are presented as the mean ± SD of at least three repeats and were compared using a one-way ANOVA followed by Bonferroni's correction. *P<0.05, **P<0.01, ****P<0.0001. APAP, acetaminophen; H&E, hematoxylin and eosin; IHC, immunohistochemistry; ALT, alanine aminotransferase; AST, aspartate aminotransferase; SREBP-1, sterol regulatory element-binding protein 1; PPAR-α, peroxisome proliferator-activated receptor α; Fasn, fatty acid synthase; iNOS, inducible nitric oxide synthase; NOX4, NADPH oxidase 4.

to liver diseases. For example, a study indicated that p38γ could regulate the proliferation of HCC cells (22). However, the role of p38γ as a therapeutic target for APAP-induced liver injury remains poorly understood. Based on the preliminary research of our previous studies and the core role of inflammation, oxidative stress and lipid metabolism disorders in APAP-induced liver injury, p38γ was focused on for further study among the significantly upregulated genes. Of note, the results showed that p38γ expression was upregulated in APAP-treated AML-12 cells (Fig. 2A-C). The upregulation of p38γ provides a very reasonable and novel mechanism connection between APAP-induced liver injury (associated with oxidative stress, lipid buildup and inflammatory responses) and the molecular regulatory network mediated by p38γ. The results of the GO enrichment analysis showed that the liver injury induced by APAP was linked to oxidative stress, lipid buildup and inflammatory responses (Fig. 2D). Double immunofluorescence staining showed that p38γ co-localized with hepatocyte albumin in the liver tissues (Fig. 2E), suggesting that p38γ was expressed in hepatocytes.

In addition, immunofluorescence, RT-qPCR and western blot analysis results showed that the p38γ expression level was significantly increased in the liver tissues of APAP-treated mice compared with the normal group (Fig. 2F, G and I). Similarly, p38γ expression was also upregulated in APAP-treated AML-12 cells (Fig. 2F, H and J). Collectively, these findings from both *in vivo* (APAP-treated mice) and *in vitro* (APAP-treated AML-12 cells) models confirmed that APAP successfully induced liver injury and consistently demonstrated p38γ upregulation in this APAP-induced liver injury model, suggesting that p38γ is functionally involved in the pathogenesis of APAP-induced liver injury. Thus, the specific role of p38γ in this process was further investigated.

p38γ regulates APAP-induced oxidative stress and lipid accumulation in AML-12 cells. A growing body of evidence underscores the importance of oxidative stress and lipid accumulation in liver injury induced by APAP (46-48). Thus, whether p38γ is functionally involved in regulating oxidative stress and lipid accumulation was next assessed. To this end, the p38γ-siRNA and pEGFP-C1-p38γ were used to downregulate and upregulate p38γ expression, respectively. Satisfactory transfection efficiency was obtained at 24 h post-transfection (Figs. S2A-D and S3C). Next, it was found that the MDA level was increased, while the GSH and SOD levels were decreased in APAP-induced AML-12 cells compared with normal cells. p38γ knockdown reduced MDA levels and increased the levels of GSH and SOD. By contrast, overexpression of p38γ increased MDA levels and decreased the GSH and SOD levels (Fig. 3A-C). Oil red O staining showed accumulation of cellular lipid in APAP-treated AML-12 cells compared with the normal group. Lipid accumulation was reduced by p38γ knockdown compared with p38γ NC treatment, whereas overexpression of p38γ resulted in increased lipid accumulation (Fig. 3D). The results of DCF, DHE and MitoSOX staining revealed increased ROS production within the APAP group compared with the normal group. Downregulation of p38γ inhibited the production of ROS compared with the APAP + p38γ NC group. Conversely, ROS generation was increased following p38γ overexpression compared with the APAP + pEGFP-C1 group (Fig. 3E). Next, the expression levels of SREBP-1, Fasn and PPAR-α were assessed, three proteins that are linked to lipogenesis (49). The results showed that APAP treatment increased the expression of SREBP-1 and Fasn, and decreased the expression of PPAR-α. The effect of APAP treatment on these lipid accumulation-related proteins was promoted by pEGFP-C1-p38γ (Fig. 3G) and reduced by p38γ siRNA (Fig. 3F). The expression levels of oxidative stress-related proteins (iNOS and NOX4) in AML-12 cells were assessed; their expression was increased in APAP-induced AML-12 cells. p38γ overexpression increased the impact of APAP treatment on the production of NOX4 and iNOS (Fig. 3G), whereas p38γ knockdown reduced their expression (Fig. 3F), indicating the regulatory function of p38γ in oxidative stress. Overall, these results demonstrated that p38γ increased oxidative stress and lipid accumulation aggravated by APAP in liver injury.

p38γ regulates APAP-induced inflammatory response in AML-12 cells. Inflammation is a critical cause of APAP-induced hepatic injury. Therefore, the impact of p38γ on the inflammatory response in APAP-treated AML-12 cells was next assessed. The ELISA results indicated that the expression of TNF-α, IL-6 and IL-1β were elevated by APAP. This increase in inflammatory cytokine release was significantly suppressed by p38γ knockdown and enhanced by p38γ overexpression (Fig. 4A and B). Furthermore, the results of the RT-qPCR analysis showed that, after p38γ-siRNA treatment, the expression levels of IL-1β, TNF-α and IL-6 were significantly downregulated (Fig. 4C). However, p38γ overexpression significantly increased the expression levels of IL-1β, TNF-α and IL-6 (Fig. 4D). Notably, these results were further validated through western blot analysis (Fig. 4E and F). Consequently, these findings provided evidence supporting the involvement of p38γ in the release of inflammatory cytokines during APAP-induced liver injury.

miR-125 directly targets p38γ in AML-12 cells. TargetScan was used to determine the upstream regulatory mechanism of p38γ. TargetScan analysis showed that a large number of miRNAs could target the 3'-UTR region of p38γ, such as miR-4319. However, among all the predicted miRNAs targeting p38γ, miR-125 had a very high 'context++ score', which is a key indicator reflecting binding affinity and conservation, and identified miR-125 as a regulator targeting the 3'-UTR of p38γ (Fig. 5A). To further investigate if the predicted binding site of miR-125 to the 3'-UTR of p38γ mRNA was responsible for the downregulation of p38γ, a WT and MUT 3'-UTR of p38γ was cloned into a luciferase reporter vector. WT-p38γ and miR-125 mimics or scrambled control were co-transfected into AML-12 cells to perform a luciferase reporter assay. In AML-12 cells transfected with miR-125 mimics, the luciferase activity was significantly reduced compared with the scrambled control cells (Fig. 5B). In addition, the miR-125 mimics and miR-125 inhibitor were used to upregulate and downregulate the miR-125 expression, respectively. Satisfactory transfection efficiency was obtained at 24 h post-transfection (Fig. S3A-D). RT-qPCR results indicated that the mRNA level of p38γ was downregulated by miR-125 mimics and upregulated by miR-125 inhibitor (Fig. 5C); western blot analysis further validated these findings (Fig. 5D). Next, AML-12 cells were

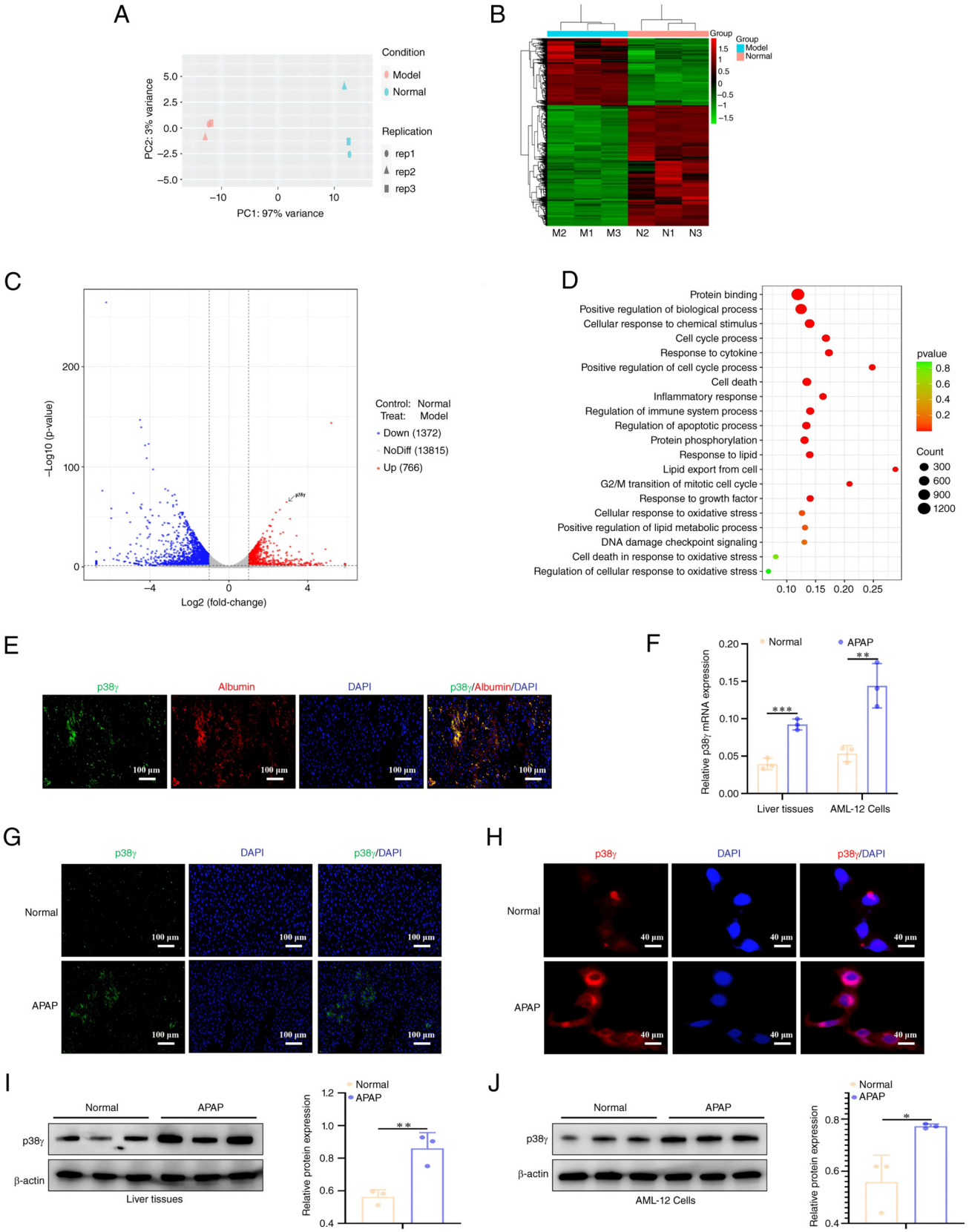

Figure 2. p38γ expression is increased in APAP-induced liver injury. (A) PCA results of RNA-sequencing analysis. (B) Heatmap showing changes in protein levels between AML-12 cells and AML-12 cells after treatment with APAP. (C) Volcano plot showing changes in protein levels between AML-12 cells and AML-12 cells after treatment with APAP. (D) Gene Ontology was used for pathway enrichment analysis of differentially expressed genes in APAP-indued AML-12 cells. (E) Double immunofluorescence staining of p38γ and albumin from APAP-induced mice liver injury; scale bar, 100 μm. (F) Reverse transcription-quantitative PCR analysis of p38γ mRNA expression in liver tissues and AML-12 cells; mRNA expression was normalized to GAPDH. (G) Immunofluorescence staining of p38γ in APAP-induced mice liver injury samples; scale bar, 100 μm. (H) Immunofluorescence staining of p38γ in AML-12 cells; scale bar, 40 μm. Representative western blots and densitometry analysis of p38γ expression in (I) liver extracts prepared from APAP-induced mice liver tissues and (J) AML-12 cells. Data are presented as the mean ± SD of at least three repeats and were compared using a one-way ANOVA followed by Bonferroni's correction. *P<0.05, **P<0.01, ***P<0.001. APAP, acetaminophen; PCA, principal component analysis.

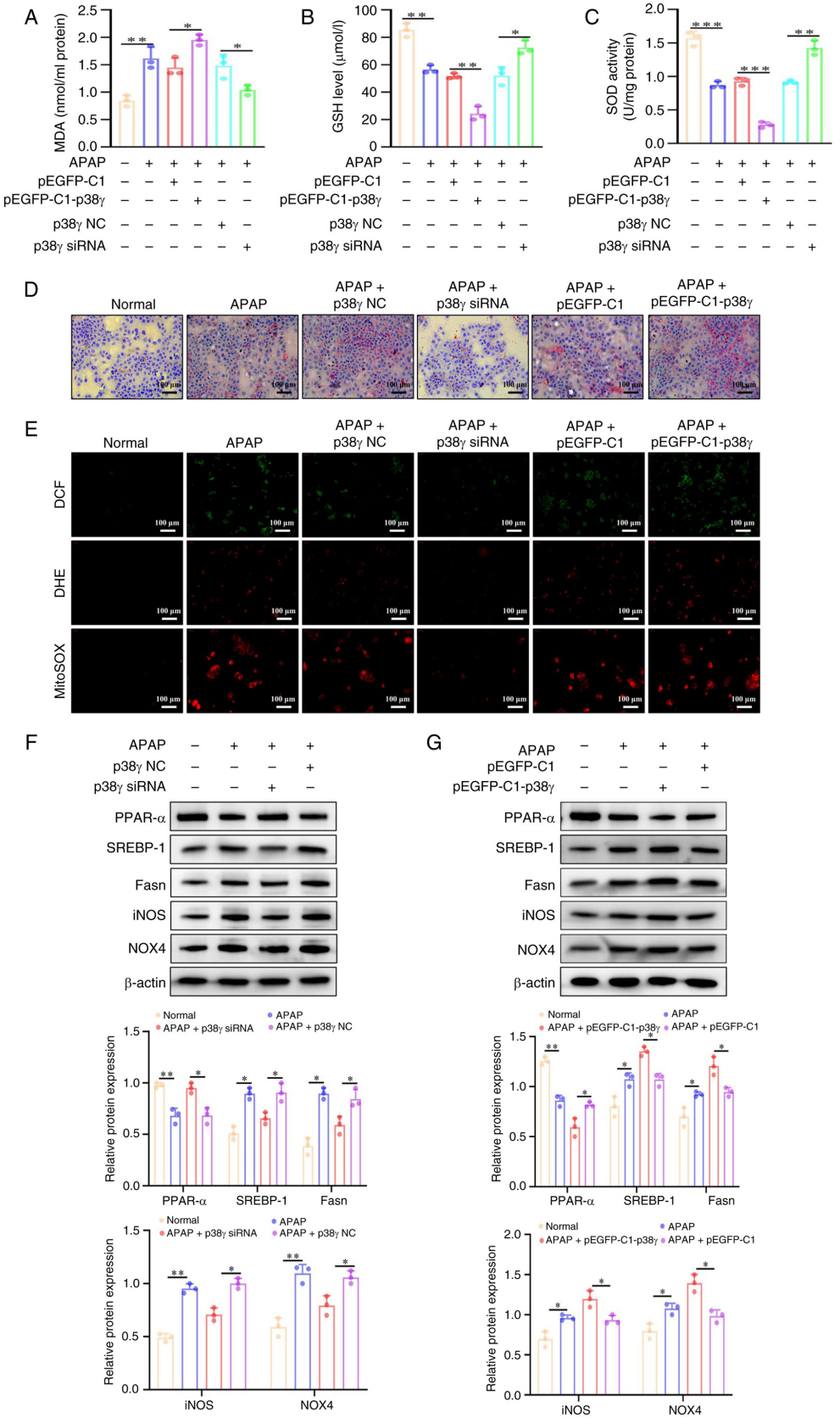

Figure 3. p38γ knockdown inhibits oxidative stress and lipid accumulation in APAP-induced AML-12 cells. Intracellular (A) MDA, (B) GSH and (C) SOD activities were assayed in AML-12 cells transfected with p38γ siRNA and pEGFP-C1-p38γ according to the manufacturer's instructions (n=3). (D) Representative images of Oil red O staining of AML12 cells transfected with p38γ siRNA and pEGFP-C1-p38γ; scale bar, 100 μm. (E) Reactive oxygen species production was detected by DCF, DHE and MitoSOX assay after overexpression and knockdown of p38γ. Western blot analysis of PPAR-α, SREBP-1, Fasn, iNOS and NOX4 expression in AML-12 cells following p38γ (F) knockdown and (G) overexpression. Data are presented as the mean ± SD of at least three repeats and were compared using a one-way ANOVA followed by Bonferroni's correction. *P<0.05, **P<0.01, ***P<0.001. APAP, acetaminophen; MDA, malondialdehyde; GSH, glutathione; SOD, superoxide dismutase; siRNA, small interfering RNA; NC, negative control; DCF, 2',7'-dichlorofluorescein; DHE, dihydroethidium; PPAR-α, peroxisome proliferator-activated receptor α; SREBP-1, sterol regulatory element-binding protein 1; Fasn, fatty acid synthase; iNOS, inducible nitric oxide synthase; NOX4, NADPH oxidase 4.

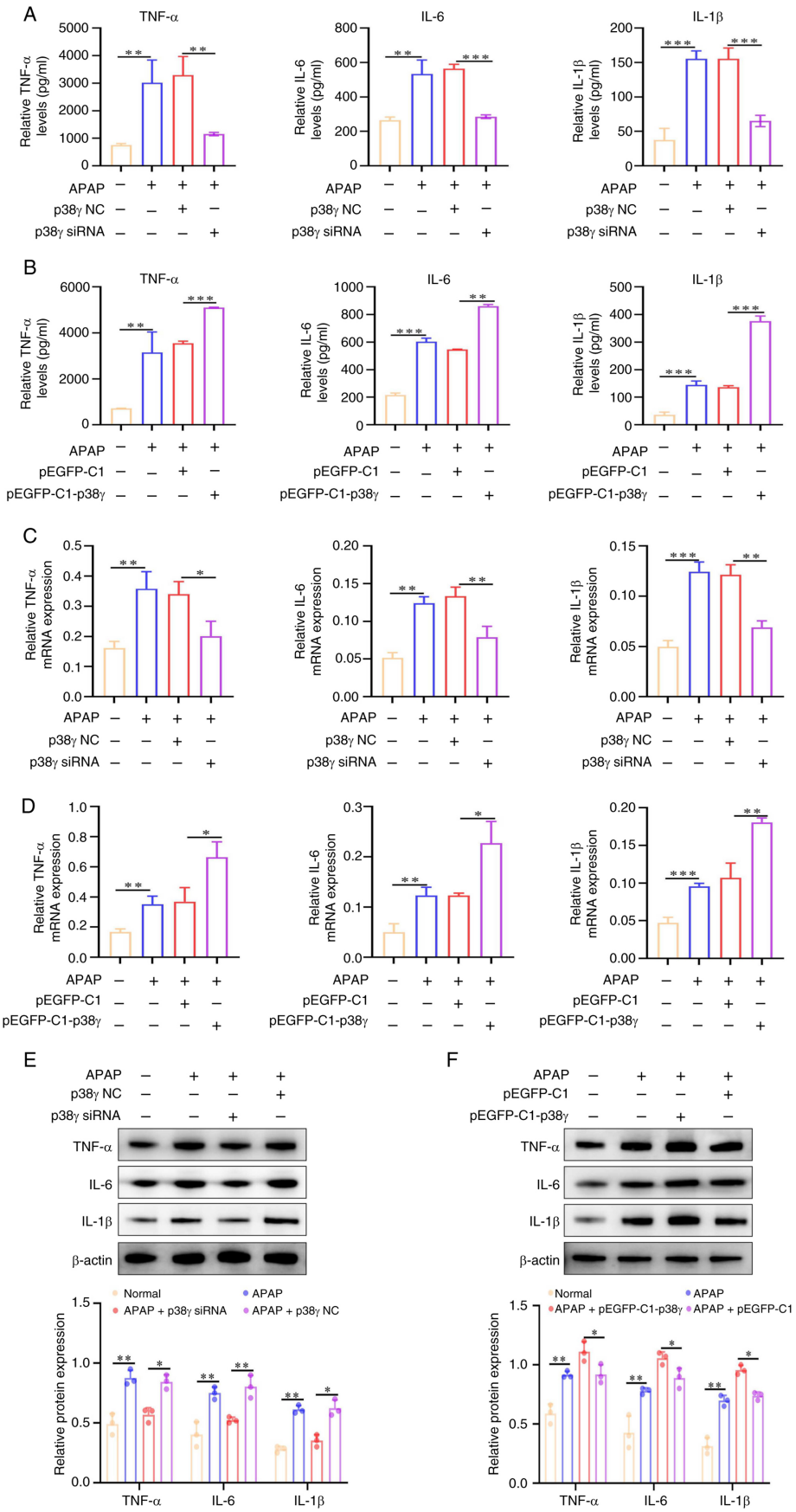

Figure 4. p38γ knockdown inhibits inflammatory responses in APAP-induced AML-12 cells. (A) TNF-α, IL-6 and IL-1β expression was assessed by ELISA in AML-12 cells transfected with p38γ siRNA. (B) TNF-α, IL-6 and IL-1β expression was assessed by ELISA in AML-12 cells transfected with pEGFP-C1-p38. Reverse transcription-quantitative PCR analysis of TNF-α, IL-6 and IL-1β activity in AML-12 cells following p38γ (C) knockdown and (D) overexpression. Western blot analysis of TNF-α, IL-6 and IL-1β activity in AML-12 cells following p38γ (E) knockdown and (F) overexpression. Data are presented as the mean ± SD of at least three repeats and were compared using a one-way ANOVA followed by Bonferroni's correction. *P<0.05, **P<0.01, ***P<0.001. APAP, acetaminophen; siRNA, small interfering RNA; NC, negative control.

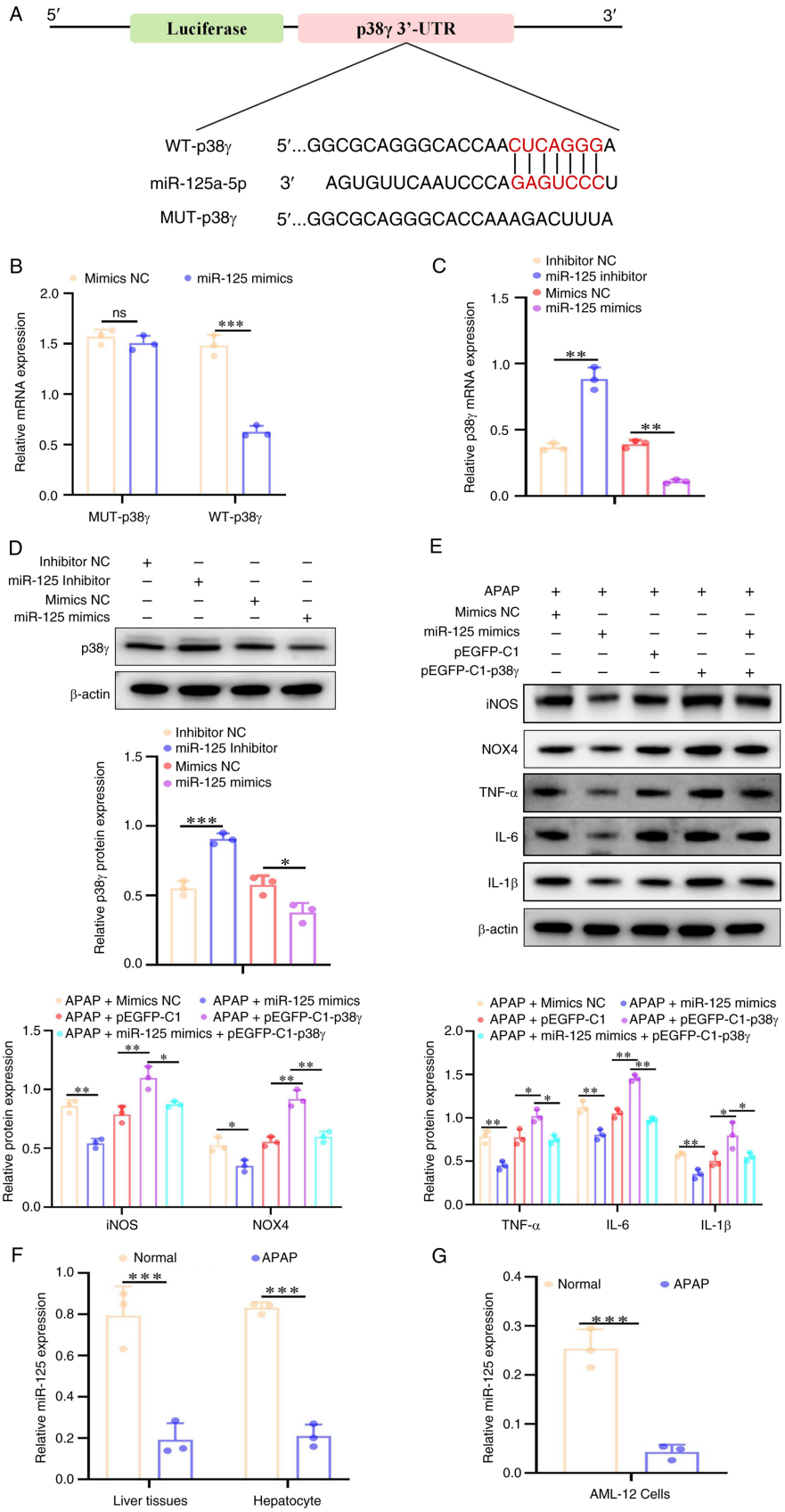

Figure 5. p38γ is a direct target of miR-125. (A) TargetScan was used to predict that p38γ possesses binding sites for miR-125. (B) A luciferase reporter assay was performed to detect luciferase activity in the mimics NC + MUT p38γ, miR-125 mimics + MUT p38γ, mimics NC + WT p38γ and miR-125 mimics + WT p38γ groups. (C) The mRNA levels of p38γ in cells were determined by RT-qPCR. (D) Western blot analysis of p38γ expression in AML-12 cells treated with miR-125 inhibitor or miR-125 mimics. (E) Western blot analysis of iNOS, NOX4, TNF-α, IL-6 and IL-1β expression in AML-12 cells. (F) The miR-125 expression was determined by RT-qPCR in liver injury tissues and primary hepatocytes. (G) miR-125 expression were determined by RT-qPCR in AML-12 cells. Data are presented as the mean ± SD of at least three repeats and were compared using a one-way ANOVA followed by Bonferroni's correction. *P<0.05, **P<0.01, ***P<0.001. ns, not significant; miR-125, microRNA-125; NC, negative control; MUT, mutant; WT, wild type; RT-qPCR, reverse transcription quantitative PCR; iNOS, inducible nitric oxide synthase; NOX4, NADPH oxidase 4; UTR, untranslated region; APAP, acetaminophen.

co-transfected with pEGFP-C1-p38γ and miR-125 mimics. Western blot analysis demonstrated a significant decrease in TNF-α, IL-6 and IL-1β protein levels in the co-transfection compared with the pEGFP-C1-p38γ transfected group (Fig. 5E). The expression levels of miR-125 in APAP-induced liver injury mice were assessed using RT-qPCR; miR-125 expression was decreased in primary hepatocytes and liver tissues (Fig. 5F). Similarly, APAP treatment significantly suppressed miR-125 expression in AML-12 cells (Fig. 5G). Taken together, these results indicated that miR-125 directly targeted the 3'-UTR regions of p38γ to inhibit its expression.

miR-125 regulates APAP-induced oxidative stress and lipid accumulation of AML-12 in liver cells by targeting p38γ. To explore the effect of miR-125 on the etiology and progression of liver injury induced by APAP treatment, additional analysis on the impact of miR-125 on indicators associated with oxidative stress and lipid accumulation was performed. The results demonstrated that knockdown of miR-125 increased MDA levels and decreased GSH and SOD levels. Notably, the increase in MDA levels and decrease in GSH and SOD levels could be reversed by the downregulation of p38γ (Fig. 6A-C). Conversely, the MDA level was reduced and the GSH and SOD levels were elevated in AML-12 cells transfected with miR-125 mimics compared with AML-12 cells transfected with mimics NC. However, the MDA level was increased and the GSH and SOD levels were decreased in AML-12 cells transfected with miR-125 mimics and pEGFP-C1-p38γ compared with AML-12 cells transfected with miR-125 mimics (Fig. 6A-C). Furthermore, the results of Oil red O staining showed that knockdown of miR-125 increased lipid accumulation compared with AML-12 cells treated with miR-NC. When AML-12 cells were treated with miR-125 inhibitor and p38γ-siRNA, lipid accumulation was reduced compared with AML-12 cells treated with miR-125 inhibitor. In addition, lipid accumulation was repressed by miR-125 overexpression and reversed by p38γ overexpression (Fig. 6D). The findings of the DCF, DHE and MitoSOX staining indicated that the generation of ROS was increased in AML-12 cells transfected with miR-125 inhibitor and decreased in AML-12 cells transfected with miR-125 mimics. However, the increase and decrease in ROS generation were reversed by p38γ-siRNA and pEGFP-C1-p38γ, respectively (Fig. 6E). Next, the expression levels of SREBP-1, Fasn and PPAR-α we evaluated. The results suggested that APAP suppressed the expression of PPAR-α and promoted the expression of SREBP-1 and Fasn. Overexpression of miR-125 increased the expression of PPAR-α and decreased the expression of SREBP-1 and Fasn. Knockdown of miR-125 significantly increased the expression of SREBP-1 and Fasn, and inhibited the expression of PPAR-α. However, the effect of miR-125 inhibitor and miR-125 mimics treatment on lipid accumulation-related proteins (PPAR-α, SREBP-1 and Fasn) was reversed by pEGFP-C1-p38γ and p38γ-siRNA, respectively (Fig. 6F and G). The expression levels of oxidative stress-related proteins (iNOS and NOX4) in AML-12 cells were next detected. It was found that the expression of iNOS and NOX4 were increased by knockdown of miR-125, and this was reversed by p38γ knockdown. By contrast, overexpression of miR-125 reduced the expression of iNOS and NOX4, and upregulation of p38γ reversed the inhibition (Fig. 6F and G), suggesting the regulatory role of miR-125 in oxidative stress. Overall, these results indicated that miR-125 primarily targeted p38γ, inhibiting the aggravation of oxidative stress and lipid accumulation in APAP-induced liver injury.

miR-125 regulates APAP-induced inflammatory response of AML-12 in liver cells by targeting p38γ. This regulatory axis was next examined in the context of inflammation. ELISA, RT-qPCR and western blotting were used in APAP-treated AML-12 cells to investigate the impact of miR-125 on inflammatory responses. Consistent with prior observations, ELISA results confirmed elevated expression levels of TNF-α, IL-6 and IL-1β following APAP treatment. However, knockdown of miR-125 significantly increased the levels of TNF-α, IL-6 and IL-1β in AML-12 cells induced by APAP, which was reversed by transfection with p38γ siRNA (Fig. 7A). Overexpression of miR-125 suppressed the levels of TNF-α, IL-6 and IL-1β, which was reversed by transfection with pEGFP-C1-p38γ in AML-12 cells treated with APAP (Fig. 7B). Furthermore, RT-qPCR results showed that knockdown of miR-125 increased the expression levels of IL-1β, TNF-α and IL-6; however, p38γ-siRNA decreased the production of these inflammatory cytokines. By contrast, overexpression of miR-125 decreased the expression levels of IL-1β, TNF-α and IL-6, but pEGFP-C1-p38γ increased the production of these inflammation cytokines (Fig. 7C and D). Furthermore, the validity of these findings was confirmed through the utilization of western blot analysis (Fig. 7E and F). In summary, these results provide evidence that, in the setting of APAP-induced liver damage, miR-125 may directly target p38γ to inhibit the production of inflammatory cytokines.

miR-125 regulates APAP-induced liver injury by targeting p38γ via the PI3K/Akt signaling pathway. The KEGG pathway enrichment analysis of the aforementioned RNA-seq data revealed the emergence of the 'PI3K-Akt signaling pathway' (Fig. 8A), suggesting that this pathway may play a role in APAP-induced liver damage. Based on these results, western blot analysis confirmed that APAP could promote the phosphorylation of PI3K and Akt (Fig. 8B and C). The expression levels of p-PI3K and p-Akt were markedly decreased by downregulating p38γ and overexpressing miR-125 (Fig. 8D and F). By contrast, upregulation of p38γ and knockdown of miR-125 significantly increased the expression levels of p-PI3K and p-Akt (Fig. 8E and G). In APAP-induced AML-12 cells, LY294002 (40 μM; 48 h) was used to inhibit PI3K/Akt signaling. The chemical structure of LY294002 is shown in Fig. 8H. In APAP-induced AML-12 cells, oxidative stress, lipid accumulation and inflammation-related proteins were detected. The results of the western blot analysis showed that the APAP + p38γ NC+ LY294002 group had higher expression levels of PPAR-α and lower expression levels of SREBP-1, Fasn, iNOS, NOX4, TNF-α, IL-6 and IL-1β compared to the p38γ NC group (Figs. 8I and 9C). The APAP + miR-125 NC + LY294002 group had higher expression levels of PPAR-α and lower expression levels of SREBP-1, Fasn, iNOS, NOX4, TNF-α, IL-6 and IL-1β compared with the miR-125 NC group (Figs. 8B and 9F). Conversely, LY294002 treatment did not further alter the expression levels of PPAR-α, SREBP-1, Fasn, iNOS, NOX4, TNF-α, IL-6 and IL-1β in the p38γ siRNA or

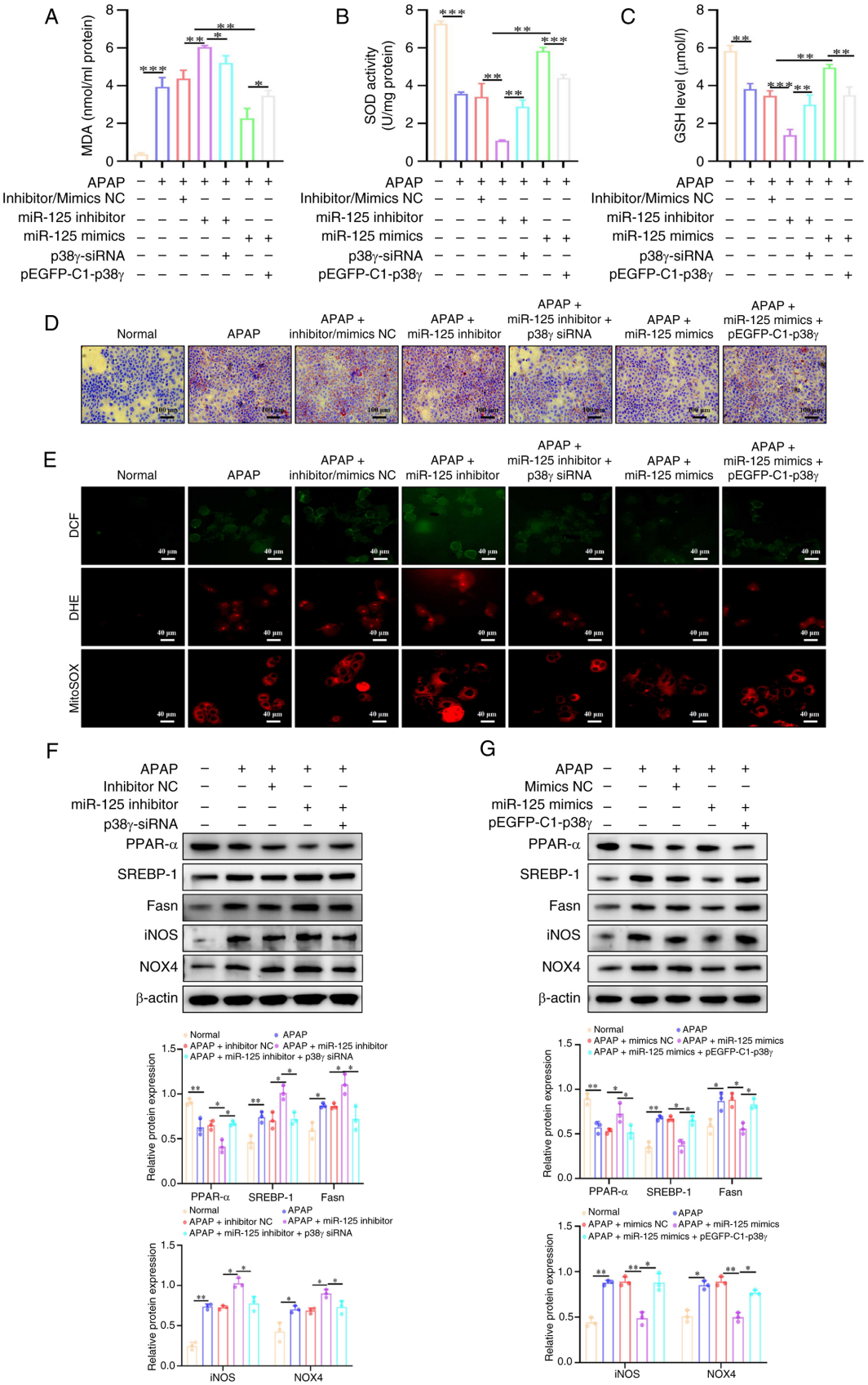

Figure 6. miR-125 inhibits oxidative stress and lipid accumulation by targeting p38γ. Intracellular levels of (A) MDA and (C) GSH and (B) activity of SOD were assessed in AML-12 cells. (D) Representative images of Oil red O staining of AML12 cells; scale bar, 100 μm. (E) Reactive oxygen species production was detected using DCF, DHE and MitoSOX assays following overexpression and knockdown of miR-125. Western blot analysis of PPAR-α, SREBP-1, Fasn, iNOS and NOX4 activity in AML-12 cells treated with (F) miR-125 inhibitor and (G) miR-125 mimics. Data are presented as the mean ± SD of at least three repeats and were compared using a one-way ANOVA followed by Bonferroni's correction. *P<0.05, **P<0.01, ***P<0.001. APAP, acetaminophen; miR-125, microRNA-125; NC, negative control; siRNA, small interfering RNA; MDA, malondialdehyde; GSH, glutathione; SOD, superoxide dismutase; DCF, 2',7'-dichlorofluorescein; DHE, dihydroethidium; PPAR-α, peroxisome proliferator-activated receptor-α; SREBP-1, sterol regulatory element-binding protein 1; Fasn, fatty acid synthase; iNOS, inducible nitric oxide synthase; NOX4, NADPH oxidase 4.

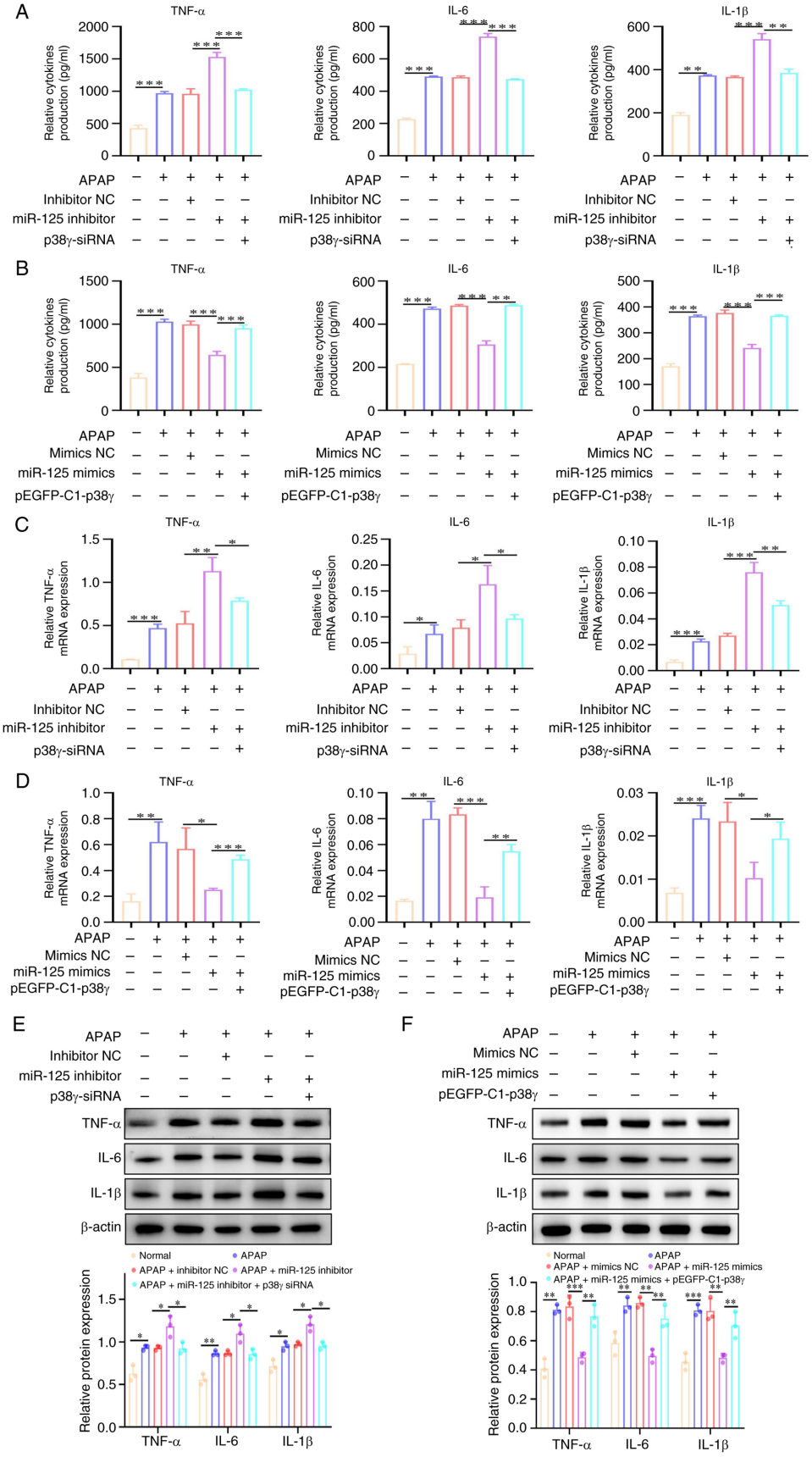

Figure 7. miR-125 inhibits inflammatory response by targeting p38γ. TNF-α, IL-6 and IL-1β levels were measured in cell supernatant using ELISA kits in AML-12 cells following (A) miR-125 knockdown along with p38γ knockdown and (B) miR-125 overexpression along with p38γ overexpression. The mRNA levels of TNF-α, IL-6 and IL-1β in AML-12 cells were determined by reverse transcription-quantitative PCR in AML-12 cells following (C) miR-125 knockdown along with p38γ knockdown and (D) miR-125 overexpression along with p38γ overexpression. Western blot analysis of TNF-α, IL-6 and IL-1β activity in AML-12 cells in AML-12 cells following (E) miR-125 knockdown along with p38γ knockdown and (F) miR-125 overexpression along with p38γ overexpression. Data are presented as the mean ± SD of at least three repeats and were compared using a one-way ANOVA followed by Bonferroni's correction. *P<0.05, **P<0.01, ***P<0.001. APAP, acetaminophen; miR-125, microRNA-125; NC, negative control; siRNA, small interfering RNA.

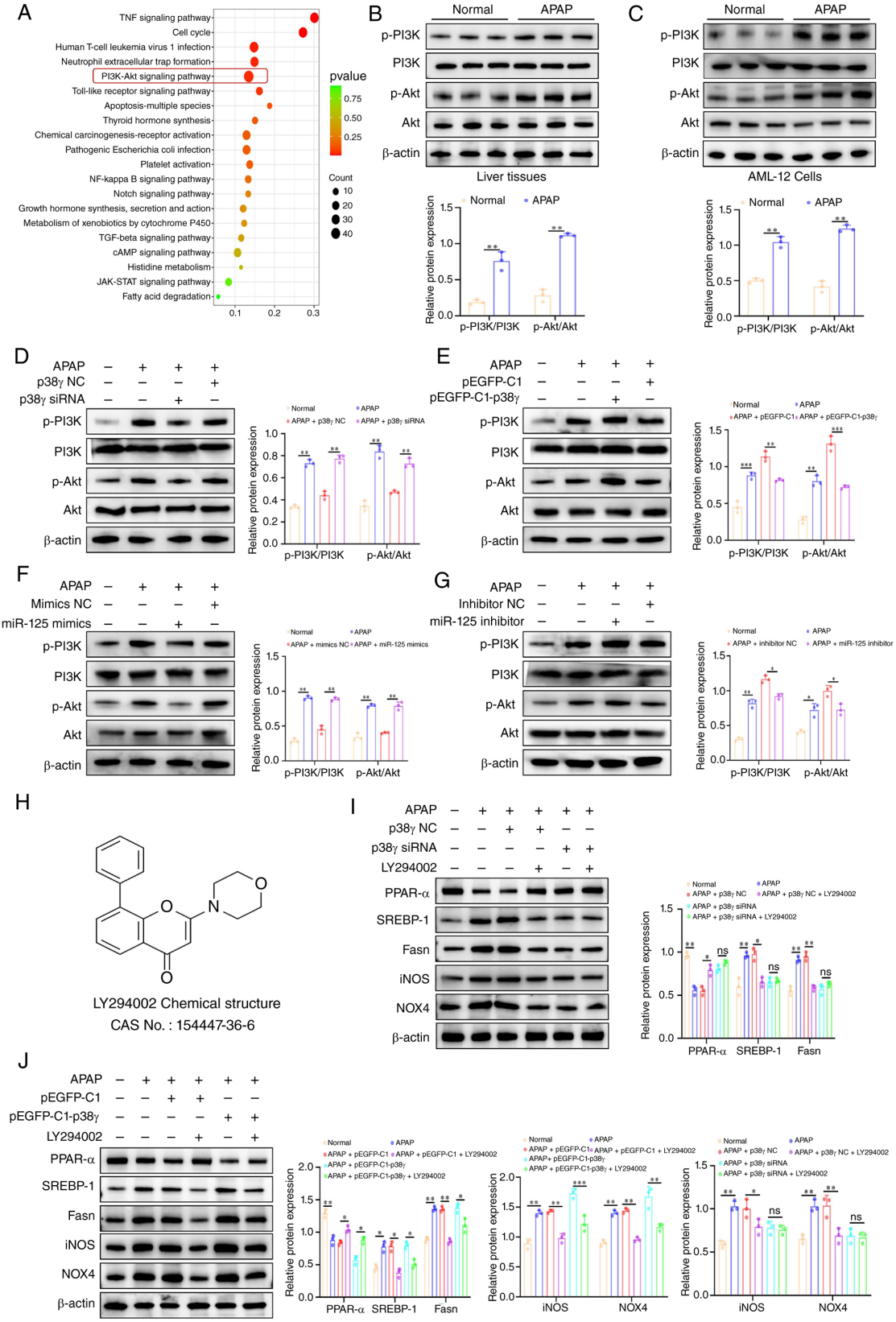

Figure 8. miR-125 reverses APAP-induced liver injury by targeting p38γ via activation of the PI3K/AKT signaling. (A) Kyoto Encyclopedia of Genes and Genomes enrichment of the potential signaling pathways associated with significantly differentially expressed genes between the control and APAP-treated groups. Western blot analysis of p-PI3K and p-AKT expression in (B) liver injury tissues and (C) AML-12 cells. Western blot analysis of p-PI3K and p-AKT expression in AML-12 cells transfected with (D) p38γ siRNA and (E) pEGFP-C1-p38γ. Western blot analysis of p-PI3K and p-AKT expression in AML-12 cells following (F) overexpression and (G) knockdown of miR-125. (H) Chemical structure of the PI3K/AKT signaling pathway inhibitor, LY294002. (I) Western blot analysis of PPAR-α, SREBP-1, Fasn, iNOS and NOX4 activity in AML-12 cells following p38γ knockdown and treatment with LY294002. (J) Western blot analysis of PPAR-α, SREBP-1, Fasn, iNOS and NOX4 activity in AML-12 cells following p38γ overexpression and treatment with LY294002. Data are presented as the mean ± SD of at least three repeats and were compared using a one-way ANOVA followed by Bonferroni's correction. *P<0.05, **P<0.01, ***P<0.001. APAP, acetaminophen; miR-125, microRNA-125; NC, negative control; siRNA, small interfering RNA; p-, phosphorylated; PPAR-α, peroxisome proliferator-activated receptor α; SREBP-1, sterol regulatory element-binding protein 1; Fasn, fatty acid synthase; iNOS, inducible nitric oxide synthase; NOX4, NADPH oxidase 4.

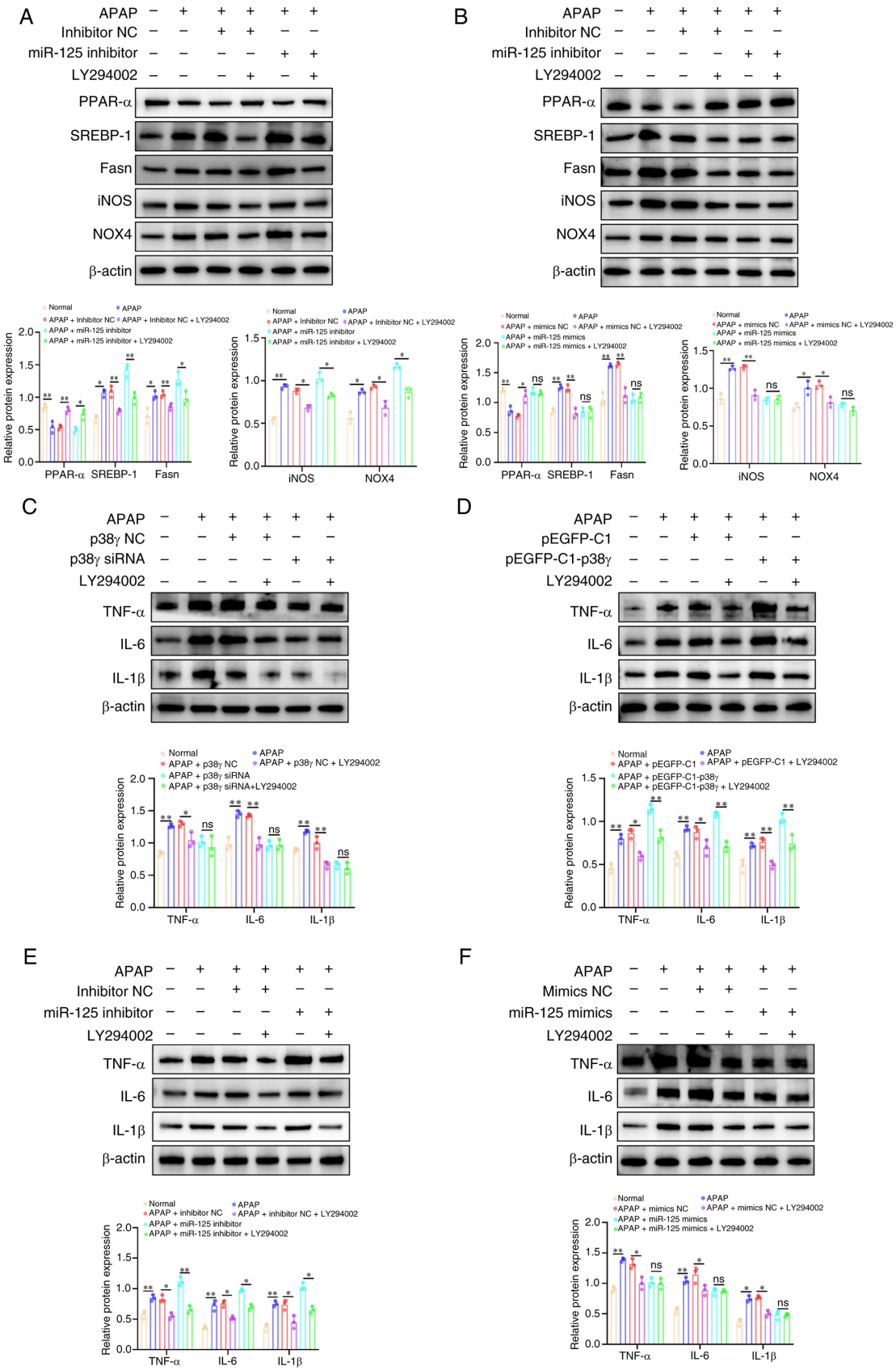

Figure 9. miR-125 reverses APAP-induced liver injury by targeting p38γ via activation of the PI3K/AKT signaling pathway. (A) Western blot analysis of PPAR-α, SREBP-1, Fasn, iNOS and NOX4 expression in AML-12 cells transfected with miR-125 inhibitor and treated with LY294002. (B) Western blot analysis of PPAR-α, SREBP-1, Fasn, iNOS and NOX4 expression in AML-12 cells transfected with miR-125 mimics and then treated with LY294002. Western blot analysis of TNF-α, IL-6 and IL-1β expression in AML-12 cells transfected with (C) p38γ siRNA and (D) pEGFP-C1-p38γ and then treated with LY294002. Western blot analysis of TNF-α, IL-6 and IL-1β expression in AML-12 cells transfected with (E) miR-125 inhibitor or (F) miR-125 mimics and then treated with LY294002. Data are presented as the mean ± SD of at least three repeats and were compared using a one-way ANOVA followed by Bonferroni's correction. *P<0.05, **P<0.01. ns, not significant; APAP, acetaminophen; miR-125, microRNA-125; NC, negative control; siRNA, small interfering RNA; PPAR-α, peroxisome proliferator-activated receptor α; SREBP-1, sterol regulatory element-binding protein 1; Fasn, fatty acid synthase; iNOS, inducible nitric oxide synthase; NOX4, NADPH oxidase 4.

miR-125 mimics group compared with the p38γ siRNA or miR-125 mimics group, indicating that the protective effects of p38γ knockdown or miR-125 overexpression are largely mediated through the PI3K/Akt signaling pathway (Figs. 8I, 9B, C and F). Conversely, compared with the pEGFP-C1/miR-125 NC group, the pEGFP-C1/miR-125 NC + LY294002 group showed decreased expression levels of SREBP-1, Fasn, iNOS, NOX4, TNF-α, IL-6 and IL-1β, and increased expression levels of PPAR-α. However, the pEGFP-C1-p38γ/miR-125 inhibitor + LY294002 group exhibited repressed expression levels of SREBP-1, Fasn, iNOS, NOX4, TNF-α, IL-6 and IL-1β, and elevated expression levels of PPAR-α compared to the pEGFP-C1-p38γ/miR-125 inhibitor group (Figs. 8J, 9A, D and E). These results suggested that miR-125 may inhibit oxidative stress, lipid accumulation and inflammatory response by targeting p38γ via the PI3K/Akt signaling pathway in APAP-induced liver injury.

p38γ knockdown attenuates liver injury induced by APAP in mice. AAV9-shRNA-p38γ was injected into the tail vein to knock down p38γ expression to investigate the possible role of p38γ in APAP-induced liver injury in more detail. The results showed that the p38γ knockout mice were successfully constructed (Fig. 10A and B). Immunofluorescence and western blot results indicated that AAV9-shRNA-p38γ reduced the expression level of p38γ (Fig. 10C and D). H&E staining results showed that inflammatory cell infiltration, vacuolar degeneration and the area of necrosis were significantly decreased, indicating liver injury was reduced in AAV9-shRNA-p38γ mice (Fig. 10E). IHC staining results showed that the expression of TNF-α, IL-6 and IL-1β were decreased in the AAV9-shRNA-p38γ mice (Fig. 10F). In addition, the AAV9-shRNA-p38γ group showed higher serum GSH and SOD levels compared with the AAV9-Empty group (Fig. 10I and K). By contrast, the serum levels of ALT, AST and MDA were lowered (Fig. 10G, H and J). Oil red O staining suggested that the lipid accumulation was decreased in the AAV9-shRNA-p38γ group (Fig. 10L). Crucially, primary hepatocytes were extracted from both the AAV9-shRNA-p38γ group and the AAV9-Empty group. The DFH staining findings indicated that the generation of ROS was reduced in the AAV9-shRNA-p38γ group (Fig. 10M). Additionally, the expression of PPAR-α was increased in the AAV9-shRNA-p38γ group; however, the expression of SREBP-1, Fasn, iNOS, NOX4, TNF-α, IL-6 and IL-1β was suppressed, according to the findings of the western blot analysis (Fig. 10N and O). Collectively, these findings indicate that the notable impacts of hepatic p38γ depletion are partially governed by the reduction of APAP-induced inflammation, oxidative stress and lipid accumulation. Essentially, miR-125 may regulate p38γ, which may function as an important modulator in the setting of APAP-induced liver damage.

Discussion

Although the role of p38γ in hepatic pathophysiology has been previously investigated, including in combined ethanol and APAP injury models (27), the present study was the first to reveal a novel comprehensive regulatory axis specific to APAP overdose. The present study noted several key advances: Firstly, the study focused on APAP hepatotoxicity, which is the leading cause of acute liver failure in a number of countries worldwide (50); secondly, and most notably, it was verified that miR-125 is a direct upstream regulator of p38γ using luciferase reporter gene assays; thirdly, it was demonstrated that the detrimental effects of p38γ may be mediated through activation of the PI3K/Akt signaling pathway; and finally, through AAV9-mediated *in vivo* knockdown of p38γ, the therapeutic potential of targeting this pathway was confirmed. Collectively, the present study demonstrated that miR-125 downregulated the expression of p38γ and that the reduction of p38γ lead to inhibition of the PI3K/Akt signaling pathway in APAP-induced liver injury, revealing a regulatory axis for this affliction.

In the most severe instances, DILI, which is the primary cause of acute liver failure in Western nations (51), can result in liver necrosis or fatality. Drug-induced hepatotoxicity can manifest as either common (predictable), such as in the case of APAP, or as idiosyncratic (unpredictable) (52). APAP, a widely utilized antipyretic, analgesic and anti-inflammatory medication, is commonly prescribed in clinical settings. For a healthy adult, a dose of ≤4,000 mg per day is generally considered safe and well-tolerated (53,54). Nevertheless, elevated concentrations of usage or prolonged excessive accumulation may lead to liver injury and potentially progress to liver failure. The pathogenesis of APAP hepatotoxicity is multifaceted. Briefly, APAP undergoes hepatic metabolism by the enzyme cytochrome P450 2E1, resulting in the formation of NAPQI. This metabolite is subsequently conjugated and detoxified with GSH. However, when hepatic GSH is depleted, an excess of NAPQI accumulates, leading to mitochondrial dysfunction (55). This dysfunction triggers the production of a significant quantity of ROS (56). Elevated levels of ROS can further impair the mitochondria, initiate a cycle of damage and ultimately result in hepatic impairment. Moreover, a previous study has highlighted the strong association between abnormal lipid metabolism and excessive APAP-induced liver injury in rats (11). Notably, prior research has shown that dihydromyricetin effectively mitigates APAP-induced liver injury in mice through the inhibition of p53-mediated regeneration, regulation of lipid homeostasis and APAP metabolism (57). Furthermore, it has been suggested that inflammation may exacerbate the initial damage caused by APAP (58-60), while also facilitating the elimination of deceased cells and debris, as well as promoting liver repair and regeneration during the later stages of damage (61,62). Consequently, inflammation appears to possess a distinct function throughout various phases of the pathogenic progression of APAP-induced liver injury (55). Collectively, these studies underscore the central roles of the inflammatory response, oxidative stress and lipid dysregulation in APAP-induced liver injury. One of the most commonly used animal models for APAP-induced liver damage is the mouse model, which has been used extensively to study the molecular pathways underlying APAP-induced liver injury (63,64). Accordingly, an APAP-induced liver injury model in mice was employed in the present study to investigate the role of p38γ in DILI. Of note, distinct manifestations resembling DILI following APAP administration were observed, including elevated liver enzyme levels, hepatic tissue damage, oxidative stress, inflammatory responses and

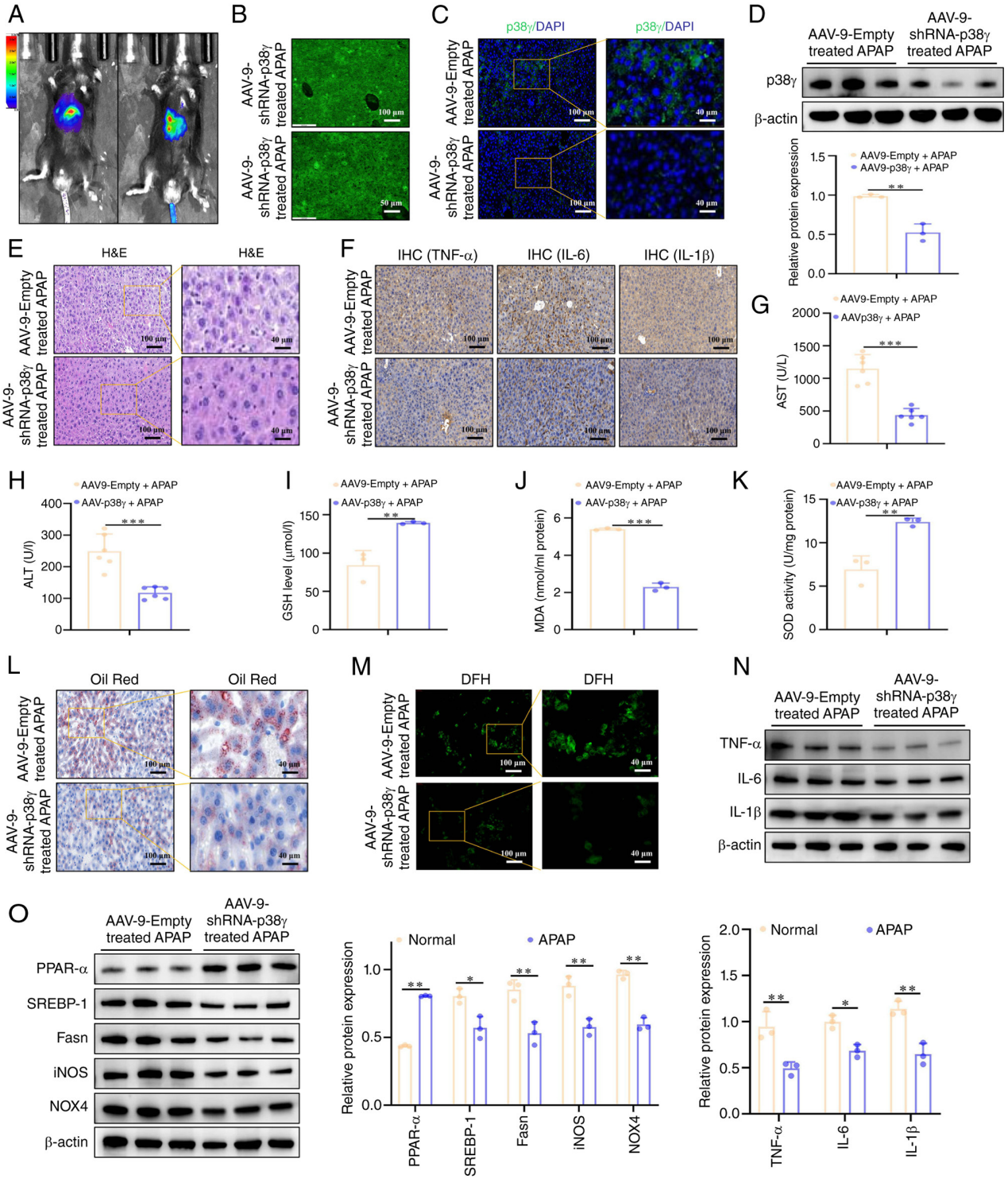

Figure 10. p38γ knockdown attenuates liver injury in APAP-treated mice. (A) Small animal imaging analysis. (B) Fluorescence imaging analysis showed that AAV9-shRNA-p38γ was specifically located in the mouse liver tissues. (C) Immunofluorescence staining of p38γ in APAP-induced mice liver injury tissues; scale bar, 100 μm. (D) Western blot analysis of p38γ expression in mouse liver tissues. (E) The H&E staining of liver sections; scale bar, 100 and 40 μm. (F) IHC analysis of TNF-α, IL-6 and IL-1β expression in liver extracts prepared from mice liver tissues. Serum levels of (G) AST and (H) ALT were measured (n=6). Serum levels of (I) GSH, (J) MDA and (K) SOD were measured (n=3). (L) Representative images of Oil red O staining of AML-12 cells; scale bar, 100 and 40 μm. (M) DCF analysis of reactive oxygen species production; scale bar, 100 and 40 μm. (N) Western blot analysis of TNF-α, IL-6 and IL-1β expression in mouse liver tissues. (O) Western blot analysis of PPAR-α, SREBP-1, Fasn, iNOS and NOX4 expression in mouse liver tissues. Data are presented as the mean ± SD of at least three repeats and were compared using a two-tailed unpaired Student's t-test. *P<0.05, **P<0.01, ***P<0.001. APAP, acetaminophen; AAV, adeno-associated virus; shRNA, short hairpin RNA; H&E, hematoxylin and eosin; IHC, immunohistochemistry; AST, aspartate aminotransferase; ALT, alanine aminotransferase; GSH, glutathione; MDA, malondialdehyde; SOD, superoxide dismutase; DFH, dihydrofluorescein; DCF, 2',7'-dichlorofluorescein; PPAR-α, peroxisome proliferator-activated receptor alpha; SREBP-1, sterol regulatory element-binding protein 1; Fasn, fatty acid synthase; iNOS, inducible nitric oxide synthase; NOX4, NADPH oxidase 4.

lipid accumulation. Subsequent knockdown of p38γ effectively mitigated APAP-induced liver injury by suppressing inflammatory response, oxidative stress and lipid accumulation.

There are four isoforms of the p38MAPK signaling pathway, each of which is encoded by a different gene: p38α, p38β, p38γ and p38δ. These isoforms are activated in response to different cellular stressors and inflammatory cytokines (65). It is noteworthy that p38α plays a critical role in immune response regulation and the generation of pro-inflammatory molecules (66). Additionally, previous studies have demonstrated the crucial involvement of p38γ in the regulation of cytokine production, T-cell activation, insulin resistance and the development of inflammation-associated tumorigenesis (30,31,67). p38γ expression is highly increased in several primary human tumor cell lines, including osteosarcoma, breast cancer, colorectal cancer and HCC (68,69). The upregulation of p38γ significantly enhances the proliferative and migratory/invasive capacities of primary cancer cells through the phosphorylation of the Rb tumor suppressor protein at the molecular level, whilst upregulating expression of the cell cycle protein cyclin E1/A (68). Moreover, stimulation of p38γ leads to cell cycle arrest in the G2/M phase and sustains the survival of cancer cells (70). Furthermore, p38γ has been linked to NAFLD in dietary rodent models. Myeloid-specific p38γ deletion has been shown to impede neutrophil migration, ameliorating steatosis and liver damage (28,66,69), highlighting p38γ as a potential therapeutic target in metabolic liver disease. The findings indicated that targeting p38γ may present a promising approach for the development of therapeutics for liver diseases. However, the specific functional roles of p38γ in liver injury remain unexplored.

In the present study, an APAP-induced liver injury mouse model was used to investigate the effect of p38γ on liver injury. The findings indicated that APAP upregulated the expression of p38γ in a dose-dependent manner. Moreover, knockdown of p38γ decreased the MDA level and increased the GSH and SOD levels, while overexpression of p38γ increased the MDA level and decreased the GSH and SOD levels. ROS production was reduced by the knockdown of p38γ and upregulated by the overexpression of p38γ. Notably, Oil red O staining showed that downregulation of p38γ notably decreased lipid accumulation and the expression of lipid metabolism-related proteins. p38γ siRNA transfection also decreased the levels of the inflammation-related proteins, TNF-α, IL-6 and IL-1β. Together, the results of the present study showed that p38γ may play a notable role in regulating hepatic inflammatory response, oxidative stress and lipid accumulation during APAP-induced liver damage. The results also suggested that p38γ suppression may be a viable therapeutic approach for the management of liver injury.

In the present study, AAV9-shRNA-p38γ was injected into the tail veins of APAP-induced liver injury mice to knock down p38γ expression. The results demonstrated that inflammatory response, oxidative stress and lipid accumulation were decreased in the AAV9-shRNA-p38γ mice compared with the AAV9-shRNA-NC mice, suggesting that the significant effect of liver p38γ depletion on APAP-induced liver injury was mainly due to its ability to alleviate the inflammatory response, oxidative stress and lipid deposition. Notably, while the results indicated that AAV9-shRNA-p38γ mainly targeted hepatocytes and achieved protective effects by knocking down p38γ expression in the liver, the possibility of minor off-target effects or systemic effects should be acknowledged. Although AAV9 has a strong liver-tending property, it cannot be completely ruled out that it may have low-level transduction in other cell types within the liver, such as Kupffer cells or sinusoidal endothelial cells, or in extracorporeal tissues. This off-target transduction may contribute to the observed phenotype through indirect mechanisms. However, multiple pieces of evidence support that the protective effect of AAV9- shRNA-p38γ is mainly mediated by the knockdown of p38γ in the liver. The specific enrichment of AAV9 in liver tissue, the most significant p38γ knockdown efficiency in the liver and the direct association between the reduction of p38γ in the liver and the reversal of the APAP-induced injury phenotype. Future studies using cell type-specific knockout models will help to ultimately confirm the cell-autonomous role of p38γ in hepatocytes in APAP-induced liver injury. Previous studies have demonstrated that p38γ promoted hepatic steatosis and inflammatory responses by modulating the JAK/STAT pathway in NAFLD models (28) and is essential for cell cycle progression and liver tumorigenesis (22). Notably, González-Terán *et al* (71) demonstrated that p38γ and p38δ were elevated in the livers of obese patients with NAFLD and that mice with myeloid cells lacking p38γ/δ are resistant to diet-induced fatty liver, hepatic triglyceride accumulation and glucose intolerance. Furthermore, Criado *et al* (31) also found that reduced disease severity in p38γ-knockdown mice was associated with lower cytokine production and anti-collagen antibody responses, indicating that p38γ may be a crucial regulator of inflammatory joint destruction in collagen-induced arthritis. These findings indicated that p38γ may be potential therapeutic target in complex diseases, such as rheumatoid arthritis, that involve innate and adaptive immune responses. Consistently, the present study also identified p38γ as a key regulator of inflammation in APAP-induced liver injury, supporting the broad role of p38γ in modulating inflammatory responses across multiple disease types. Additionally, Zhu *et al* (72) found that p38γ knockdown markedly attenuated brain tissue damage, oxidative stress and inflammatory cell infiltration in brain damage mice. In summary, the findings of these studies are consistent with the results of the present study, supporting a key role for p38γ in regulating oxidative stress, lipid metabolism and inflammation across multiple tissue and disease contexts.

In the present study, TargetScan was used to predict that p38γ may be a direct target of miR-125. miR-125 was shown to bind to the 3'-UTR of p38γ and thus regulate p38γ expression. Although TargetScan analysis predicted multiple potential miRNAs that might target p38γ, miR-125 was chosen as the focus of the present study. TargetScan analysis showed that among all the predicted miRNAs targeting p38γ, miR-125 had a very high 'context++ score', which is a key indicator reflecting binding affinity and conservation. The binding site between miR-125 and the 3'-UTR of p38γ is highly conserved across mammalian species, such as humans and mice (73). In addition, accumulating evidence has implicated miR-125 in the regulation of liver homeostasis and disease progression. For example, miR-125 was reported to be dysregulated in NAFLD, HCC and DILI (74-76), which was consistent with the focus of the present study on APAP-induced liver injury. Most notably, the results of the present study indicated that miR-125 was significantly downregulated in APAP-induced liver injury models. This concurrent dysregulation indicated

that there may be a functionally related interaction between miR-125 and p38γ in APAP-induced liver injury. These findings collectively supported miR-125 as the most promising candidate for further mechanistic exploration.

miRNAs are a highly conserved class of RNAs that regulate target mRNA by binding to its 3'-UTR and preventing the production of certain proteins (77). In previous years, numerous studies have highlighted the functional significance of specific miRNAs in various biological processes, including the dysregulation of miRNAs in the development and progression of liver disease (78,79). For instance, miR-124-3p.1 targets AKT2 and sirtuin 1 to sensitize HCC cells to sorafenib (80). In addition, Xu *et al* (81) found that miR-26a expression was induced in liver cell lines subjected to an endoplasmic reticulum stress inducer. Conversely, the hepatic expression of miR-26a was downregulated in patients with NAFLD, indicating the existence of an endoplasmic reticulum stress/miR-26a feedback loop within hepatocytes. Together, these studies support the critical role of miRNAs in regulating hepatic function and liver disease progression, consistent with the identification of miR-125 as a key regulator in APAP-induced liver injury by targeting p38γ. In the present study, miR-125 was shown to bind directly to the 3'-UTR of p38γ. miR-125 knockdown increased p38γ expression, ROS production, lipid accumulation and inflammatory cytokine secretion; these effects were reversed by p38γ knockdown. Conversely, miR-125 overexpression suppressed the expression of p38γ and its downstream effects. However, oxidative stress-related indicators and lipid accumulation-related indicators changed in the same direction under the same experimental conditions. In summary, the present study demonstrated that downregulation of miR-125 contributed to increased p38γ expression, thereby exacerbating oxidative stress, lipid accumulation and inflammation. Moreover, miR-125 may protect against APAP-induced liver injury primarily by targeting p38γ to suppress ROS production, lipid deposition and inflammatory cytokine secretion.

Based on these findings, the dynamic changes in inflammation during APAP-induced liver injury were further investigated in the present study by examining inflammatory factor expression and related signaling pathways in mouse liver tissue. It is well established that inflammation exerts a dual role in exacerbating the initial injury during t acute phase and promoting tissue repair and regeneration during the recovery phase. Although the present study did not explicitly delineate the specific roles of p38γ and miR-125 during these different stages, the upregulation of p38γ in the early stage of liver injury and the reduction in the inflammatory and oxidative stress responses caused by p38γ knockdown indicated that p38γ may primarily exacerbate disease progression during the early phase of APAP-induced liver injury. The downregulation of miR-125 during the early stage of injury may promote p38γ-driven inflammatory response. Furthermore, we hypothesize that p38γ may affect the later stages of injury repair or regeneration by modulating macrophage polarization, neutrophil clearance or hepatocyte proliferation, but this remains to be assessed. Future studies analyzing the temporal expression patterns and cell type-specific regulation of p38γ and miR-125 are required to elucidate their stage-specific contributions and therapeutic timing.

In the present study, RNA-seq analysis was performed using AML-12 cells from the normal and APAP groups. KEGG pathway enrichment analysis of the RNA-seq data showed that the PI3K/Akt signaling pathway was activated in the APAP-treated group compared with the normal control group. The PI3K pathway is of paramount importance in the regulation of cell metabolism and growth. This pathway is activated by a number of stimuli, including insulin, growth factors and cytokines; it then regulates several critical metabolic functions, including protein synthesis, lipid and glucose metabolism and energy metabolism (82,83). In addition, a recent study has hypothesized that the PI3K/Akt signaling pathway is activated in a range of diseases, leading to the activation of Akt (84). This activation of Akt subsequently triggers the activation of Bad and Caspase-9 expression, or alternatively, activates the NF-κB pathway to enhance cellular resistance against apoptosis (85,86). In the present study, it was demonstrated that APAP may activate the PI3K/Akt signaling pathway, an effect that may be enhanced by p38γ overexpression or miR-125 knockdown. By contrast, p38γ knockdown or miR-125 overexpression was shown to significantly repress the activation of the PI3K/Akt signaling pathway. Notably, LY294002 suppressed the upregulation of hepatic ROS production, lipid accumulation and inflammatory cytokine secretion, indicating that p38γ may mediate oxidative stress, lipid accumulation and inflammatory cytokine secretion during APAP-induced liver injury via the PI3K/Akt signaling pathway. Based on these findings, it is suggested that miR-125 targets p38γ to prevent hepatic oxidative stress, lipid buildup and the release of inflammatory cytokines via the PI3K/Akt pathway. However, the precise molecular mechanism by which p38γ activates the PI3K/Akt pathway remains unclear. Further investigation is required to determine whether p38γ directly phosphorylates components of the PI3K/Akt cascade or acts through intermediate adaptor proteins or upstream regulators. For example, p38γ may interact with and phosphorylate regulatory subunits of PI3K, or influence PI3K signaling by modulating the activity of phosphatases such as PTEN, which, in-turn, negatively regulate PI3K signaling. An alternative mechanism involves p38γ indirectly regulating upstream PI3K signaling by influencing the expression and activation of receptor tyrosine kinases or G protein-coupled receptors. Future studies should employ co-immunoprecipitation assays, kinase assays and phosphoproteomics to identify direct substrates of p38γ within the PI3K/Akt pathway and clarify whether its regulatory mechanism involves direct action or intermediary signaling molecules.

In summary, although previous studies have associated p38γ with inflammation-related tumorigenesis and NAFLD, the present study provides direct causal evidence that p38γ activation in hepatocytes may drive the core pathologies of APAP toxicity primarily through PI3K/Akt hyperactivation, including oxidative stress, lipid accumulation and inflammation. Notably, it was demonstrated that miR-125 may be a key upstream regulatory factor, and the absence of miR-125 explains the upregulation of p38γ during injury. To the best of our knowledge, this relationship between miR-125 and p38γ has not been reported previously. This delineation of a potential miR-125/p38γ/PI3K/Akt axis not only refines the understanding of isoform-specific p38 MAPK functions but

also highlights a potential therapeutic target for mitigating APAP-induced liver injury. Notably, in addition to miR-125, bioinformatics analysis indicated that other miRNAs might also target the 3'-UTR region of p38γ, such as miR-4319, suggesting that there are additional upstream regulatory mechanisms that can activate p38γ in APAP-induced liver injury. Although the present study focused on miR-125, future work should explore the roles of these alternative regulatory factors. Moreover, although the present study demonstrated that the PI3K/Akt signaling pathway may be a key downstream mediator of p38γ, the specific PI3K/Akt effector molecules that execute phenotypes such as oxidative stress, lipid accumulation and inflammation remain to be fully elucidated. Subsequent studies aimed at identifying these downstream targets will help to more comprehensively understand the signaling network that regulates APAP hepatotoxicity.

Although the findings of the present study suggest that targeting p38γ or modulating miR-125 hold therapeutic potential for APAP-induced liver injury, several implications and challenges need to be explicitly discussed. Targeting p38γ kinase is particularly appealing in drug development. Small-molecule inhibitors for kinases are generally more feasible to develop and administer clinically compared with nucleic acid-based therapies. Pharmacological inhibition of p38γ could serve as a standalone treatment or be combined with NAC to synergistically address both oxidative stress and inflammatory pathways. This approach may benefit patients who present outside the narrow therapeutic window of NAC or who are unresponsive to it. Additionally, miR-125 agonism (for example, using miR-125 mimics) represents another promising strategy. The results of the present study indicate that miR-125 negatively regulates p38γ and mitigates liver injury. However, the clinical translation of miRNA-based therapies faces challenges related to the efficiency of delivery, stability and off-target effects.

The present study has some limitations that should be acknowledged. Firstly, although the results of the present study indicated that hepatic p38γ plays a crucial role in exacerbating APAP-induced liver injury via the PI3K/Akt pathway following its regulation by miR-125, it is important to note that these findings are primarily based on hepatocytes. Double immunofluorescence staining confirmed that p38γ is upregulated in albumin-positive hepatocytes following APAP injury. However, whether this regulatory axis is cell-type-specific or conserved in other hepatic cell types (such as Kupffer, stellate or endothelial cells) remains to be explored. Future studies utilizing cell-type-specific knockout models or single-cell RNA-seq will help elucidate whether the miR-125/p38γ/PI3K/Akt axis operates autonomously in hepatocytes or also interacts with non-parenchymal cells. Conversely, the delivery of miR-125 mimics or inhibitors remains a significant challenge *in vivo*. Current nucleic acid delivery systems, such as liposomes and viral vectors, may pose issues regarding hepatocyte-specific targeting, potential immunogenicity and long-term safety. Moreover, miRNA therapeutics commonly face off-target effects due to partial complementarity with non-target mRNAs, which may lead to unintended consequences. Finally, while the present study demonstrated the efficacy of the miR-125/p38γ/PI3K/Akt axis as a therapeutic target in mouse models and cell lines, its translational relevance to APAP-induced liver injury in humans requires validation using human clinical samples. Analyzing p38γ and miR-125 expression in liver biopsy specimens from patients with APAP overdose may enhance the clinical relevance of the present findings. In conclusion, while the present study identified the miR-125/p38γ/PI3K/Akt axis as a promising therapeutic target for APAP-induced liver injury, addressing these limitations will be essential for future clinical translation.

Acknowledgements

No applicable.

Funding

The present study was supported by the National Natural Science Foundation of China (grant no. 82071401), Major Projects of the Ministry of Science and Technology of China (grant nos. 2021ZD0201102 and 2023YFA1800802) and the Anhui Provincial Higher Education Natural Science Research Project (grant no. 2023AH040290).

Availability of data and materials

The RNA-sequencing data generated in the present study may be found in the Sequence Read Archive under accession number PRJNA1367502 or at the following URL: https://www.ncbi.nlm.nih.gov/sra/?term=PRJNA1367502. All other data generated in the present study may be requested from the corresponding author.

Authors' contributions

HF contributed to writing the original draft, reviewing and editing the manuscript, project administration, formal analysis and conceptualization. MS and JW contributed to writing the original draft, project administration, formal analysis and conceptualization. HT contributed to writing the original draft, project administration, funding acquisition and conceptualization. JZ contributed to reviewing and editing the manuscript and formal analysis. YH contributed to project administration and carried out data visualization and used professional software for statistical and graphical analysis. HL, HZ, KG and ZR contributed to reviewing and editing the manuscript, supervision, formal analysis and conceptualization. All authors read and approved the final version of the manuscript. KG and ZR confirm the authenticity of all the raw data.

Ethics approval and consent to participate

All animal procedures were approved by the Anhui Medical University Experimental Animal Ethics Committee (approval no. LLSC20241364) and strictly adhered to the National Standard GB/T 35892-2018 (China) for Laboratory Animal Welfare.

Patient consent for publication

Not applicable.

Competing interests

The authors declare that they have no competing interests.

References

1. Macpherson AJ, Heikenwalder M and Ganal-Vonarburg SC: The liver at the nexus of host-microbial interactions. Cell Host Microbe 20: 561-571, 2016.
2. Larson AM, Polson J, Fontana RJ, Davern TJ, Lalani E, Hynan LS, Reisch JS, Schiødt FV, Ostapowicz G, Shakil AO, *et al*: Acetaminophen-induced acute liver failure: Results of a United States multicenter, prospective study. Hepatology 42: 1364-1372, 2005.
3. Lee WM, Hynan LS, Rossaro L, Fontana RJ, Stravitz RT, Larson AM, Davern TJ II, Murray NG, McCashland T, Reisch JS, *et al*: Intravenous N-acetylcysteine improves transplant-free survival in early stage non-acetaminophen acute liver failure. Gastroenterology 137: 856-864, 864.e1, 2009.
4. Manthripragada AD, Zhou EH, Budnitz DS, Lovegrove MC and Willy ME: Characterization of acetaminophen overdose-related emergency department visits and hospitalizations in the United States. Pharmacoepidemiol Drug Saf 20: 819-826, 2011.
5. Stravitz RT and Lee WM: Acute liver failure. Lancet 394: 869-881, 2019.
6. Chen Y, Liu K, Zhang J, Hai Y, Wang P, Wang H, Liu Q, Wong CCL, Yao J, Gao Y, *et al*: c-Jun NH_2-terminal protein kinase phosphorylates the Nrf2-ECH homology 6 domain of nuclear factor erythroid 2-related factor 2 and downregulates cytoprotective genes in acetaminophen-induced liver injury in mice. Hepatology 71: 1787-1801, 2020.
7. Qiu Y, Benet LZ and Burlingame AL: Identification of the hepatic protein targets of reactive metabolites of acetaminophen in vivo in mice using two-dimensional gel electrophoresis and mass spectrometry. J Biol Chem 273: 17940-17953, 1998.
8. Akakpo JY, Ramachandran A, Kandel SE, Ni HM, Kumer SC, Rumack BH and Jaeschke H: 4-Methylpyrazole protects against acetaminophen hepatotoxicity in mice and in primary human hepatocytes. Hum Exp Toxicol 37: 1310-1322, 2018.
9. Chen L, Dong J, Liao S, Wang S, Wu Z, Zuo M, Liu B, Yan C, Chen Y, He H, *et al*: Loss of Sam50 in hepatocytes induces cardiolipin-dependent mitochondrial membrane remodeling to trigger mtDNA release and liver injury. Hepatology 76: 1389-1408, 2022.
10. Du K, Ramachandran A and Jaeschke H: Oxidative stress during acetaminophen hepatotoxicity: Sources, pathophysiological role and therapeutic potential. Redox Biol 10: 148-156, 2016.
11. Dong S, Ji J, Hu L and Wang H: Dihydromyricetin alleviates acetaminophen-induced liver injury via the regulation of transformation, lipid homeostasis, cell death and regeneration. Life Sci 227: 20-29, 2019.
12. Zhao Z, Wei Q, Hua W, Liu Y, Liu X and Zhu Y: Hepatoprotective effects of berberine on acetaminophen-induced hepatotoxicity in mice. Biomed Pharmacother 103: 1319-1326, 2018.
13. Manieri E and Sabio G: Stress kinases in the modulation of metabolism and energy balance. J Mol Endocrinol 55: R11-R22, 2015.
14. Cuenda A and Rousseau S: p38 MAP-kinases pathway regulation, function and role in human diseases. Biochim Biophys Acta 1773: 1358-1375, 2007.
15. Platanias LC: Map kinase signaling pathways and hematologic malignancies. Blood 101: 4667-4679, 2003.
16. Wagner EF and Nebreda AR: Signal integration by JNK and p38 MAPK pathways in cancer development. Nat Rev Cancer 9: 537-549, 2009.
17. Qi X, Hou S, Lepp A, Li R, Basir Z, Lou Z and Chen G: Phosphorylation and stabilization of topoisomerase IIα protein by p38γ mitogen-activated protein kinase sensitize breast cancer cells to its poisons. J Biol Chem 286: 35883-35890, 2011.
18. Tang J, Qi X, Mercola D, Han J and Chen G: Essential role of p38gamma in K-Ras transformation independent of phosphorylation. J Biol Chem 280: 23910-23917, 2005.
19. Tortorella LL, Lin CB and Pilch PF: ERK6 is expressed in a developmentally regulated manner in rodent skeletal muscle. Biochem Biophys Res Commun 306: 163-168, 2003.
20. Wang XS, Diener K, Manthey CL, Wang S, Rosenzweig B, Bray J, Delaney J, Cole CN, Chan-Hui PY, Mantlo N, *et al*: Molecular cloning and characterization of a novel p38 mitogen-activated protein kinase. J Biol Chem 272: 23668-23674, 1997.
21. Gubern A, Joaquin M, Marquès M, Maseres P, Garcia-Garcia J, Amat R, González-Nuñez D, Oliva B, Real FX, de Nadal E and Posas F: The N-terminal phosphorylation of RB by p38 bypasses its inactivation by CDKs and prevents proliferation in cancer cells. Mol Cell 64: 25-36, 2016.
22. Tomás-Loba A, Manieri E, González-Terán B, Mora A, Leiva-Vega L, Santamans AM, Romero-Becerra R, Rodríguez E, Pintor-Chocano A, Feixas F, *et al*: p38γ is essential for cell cycle progression and liver tumorigenesis. Nature 568: 557-560, 2019.
23. Sabio G, Arthur JSC, Kuma Y, Peggie M, Carr J, Murray-Tait V, Centeno F, Goedert M, Morrice NA and Cuenda A: p38gamma regulates the localisation of SAP97 in the cytoskeleton by modulating its interaction with GKAP. EMBO J 24: 1134-1145, 2005.
24. Tian Y, Yuan W, Fujita N, Wang J, Wang H, Shapiro IM and Risbud MV: Inflammatory cytokines associated with degenerative disc disease control aggrecanase-1 (ADAMTS-4) expression in nucleus pulposus cells through MAPK and and NF-κB. Am J Pathol 182: 2310-2321, 2013.
25. Yin N, Qi X, Tsai S, Lu Y, Basir Z, Oshima K, Thomas JP, Myers CR, Stoner G and Chen G: p38γ MAPK is required for inflammation-associated colon tumorigenesis. Oncogene 35: 1039-1048, 2016.
26. Huang C, Zhang C, Li J, Duan Y, Tang Q and Bi F: Targeting p38γ synergistically enhances sorafenib-induced cytotoxicity in hepatocellular carcinoma. Cell Biol Toxicol 41: 35, 2025.
27. Hu S, Yao Y, Wei ZY, Wang SX, Wu YC, Hu Y, Yang CC, Min JL, Li LY, Zhou H, *et al*: Deletion of p38γ attenuates ethanol consumption- and acetaminophen-induced liver injury in mice through promoting Dlg1. Acta Pharmacol Sin 43: 1733-1748, 2022.
28. Yao Y, Luo ZP, Li HW, Wang SX, Wu YC, Hu Y, Hu S, Yang CC, Yang JF, Wang JP, *et al*: P38γ modulates the lipid metabolism in non-alcoholic fatty liver disease by regulating the JAK-STAT signaling pathway. FASEB J 37: e22716, 2023.
29. González-Terán B, Cortés JR, Manieri E, Matesanz N, Verdugo Á, Rodríguez ME, González-Rodríguez Á, Valverde ÁM, Martín P, Davis RJ and Sabio G: Eukaryotic elongation factor 2 controls TNF-α translation in LPS-induced hepatitis. J Clin Invest 123: 164-178, 2013.
30. Risco A, del Fresno C, Mambol A, Alsina-Beauchamp D, MacKenzie KF, Yang HT, Barber DF, Morcelle C, Arthur JS, Ley SC, *et al*: p38γ and p38δ kinases regulate the Toll-like receptor 4 (TLR4)-induced cytokine production by controlling ERK1/2 protein kinase pathway activation. Proc Natl Acad Sci USA 109: 11200-11205, 2012.
31. Criado G, Risco A, Alsina-Beauchamp D, Pérez-Lorenzo MJ, Escós A and Cuenda A: Alternative p38 MAPKs are essential for collagen-induced arthritis. Arthritis Rheumatol 66: 1208-1217, 2014.
32. Li LY, Yang JF, Rong F, Luo ZP, Hu S, Fang H, Wu Y, Yao R, Kong WH, Feng XW, *et al*: ZEB1 serves an oncogenic role in the tumourigenesis of HCC by promoting cell proliferation, migration, and inhibiting apoptosis via Wnt/β-catenin signaling pathway. Acta Pharmacol Sin 42: 1676-1689, 2021.
33. Yang J, Liu Q, Cao S, Xu T, Li X, Zhou D, Pan L, Li C, Huang C, Meng X, *et al*: MicroRNA-145 increases the apoptosis of activated hepatic stellate cells induced by TRAIL through NF-κB signaling pathway. Front Pharmacol 8: 980, 2018.
34. Chang YM, Chen PC, Hsu CP, Ma PF, Chen HL and Hsu SH: Loss of hepatic miR-194 promotes liver regeneration and protects from acetaminophen-induced acute liver injury. Biochem Pharmacol 195: 114862, 2022.
35. Wang X, He Y, Mackowiak B and Gao B: MicroRNAs as regulators, biomarkers and therapeutic targets in liver diseases. Gut 70: 784-795, 2021.
36. Szabo G and Bala S: MicroRNAs in liver disease. Nat Rev Gastroenterol Hepatol 10: 542-552, 2013.
37. Wang XW, Heegaard NHH and Orum H: MicroRNAs in liver disease. Gastroenterology 142: 1431-1443, 2012.
38. Ren R, He Y, Ding D, Cui A, Bao H, Ma J, Hou X, Li Y, Feng D, Li X, *et al*: Aging exaggerates acute-on-chronic alcohol-induced liver injury in mice and humans by inhibiting neutrophilic sirtuin 1-C/EBPα-miRNA-223 axis. Hepatology 75: 646-660, 2022.
39. Xu L, Yang Y, Wen Y, Jeong JM, Emontzpohl C, Atkins CL, Sun Z, Poulsen KL, Hall DR, Steve Bynon J, *et al*: Hepatic recruitment of eosinophils and their protective function during acute liver injury. J Hepatol 77: 344-352, 2022.
40. Xu XY, Hu JN, Liu Z, Zhang R, He YF, Hou W, Wang ZQ, Yang G and Li W: Saponins (ginsenosides) from the leaves of panax quinquefolius ameliorated acetaminophen-induced hepatotoxicity in mice. J Agric Food Chem 65: 3684-3692, 2017.

41. Kollias NS, Hess WJ, Johnson CL, Murphy M and Golab G: A literature review on current practices, knowledge, and viewpoints on pentobarbital euthanasia performed by veterinarians and animal remains disposal in the United States. J Am Vet Med Assoc 261: 733-738, 2023.
42. Guo H, Sun J, Li D, Hu Y, Yu X, Hua H, Jing X, Chen F, Jia Z and Xu J: Shikonin attenuates acetaminophen-induced acute liver injury via inhibition of oxidative stress and inflammation. Biomed Pharmacother 112: 108704, 2019.
43. Luo Y, Lei Y, Zhou H, Chen Y, Liu H, Jiang J, Xu C and Wu B: ARRB1 downregulates acetaminophen-induced hepatotoxicity through binding to p-eIF2α to inhibit ER stress signaling. Cell Biol Toxicol 40: 1, 2024.
44. Yang J, Xu L, Wu M, Fang H, Lu Y, Shi C, Wang Y, Jiang S, Ma Q, Li Z, *et al*: Paeonol derivative-6 attenuates inflammation by activating ZEB2 in acute liver injury. Int Immunopharmacol 91: 107235, 2021.
45. Livak KJ and Schmittgen TD: Analysis of relative gene expression data using real-time quantitative PCR and the 2(-Delta Delta C(T)) method. Methods 25: 402-408, 2001.
46. Hamada K, Wang P, Xia Y, Yan N, Takahashi S, Krausz KW, Hao H, Yan T and Gonzalez FJ: Withaferin A alleviates ethanol-induced liver injury by inhibiting hepatic lipogenesis. Food Chem Toxicol 160: 112807, 2022.
47. Ye D, Wang Y, Li H, Jia W, Man K, Lo CM, Wang Y, Lam KS and Xu A: Fibroblast growth factor 21 protects against acetaminophen-induced hepatotoxicity by potentiating peroxisome proliferator-activated receptor coactivator protein-1α-mediated antioxidant capacity in mice. Hepatology 60: 977-989, 2014.
48. Lee WM: Acetaminophen-related acute liver failure in the United States. Hepatol Res 38 (Suppl 1): S3-S8, 2008.
49. Liu C, Zhou B, Meng M, Zhao W, Wang D, Yuan Y, Zheng Y, Qiu J, Li Y, Li G, *et al*: FOXA3 induction under endoplasmic reticulum stress contributes to non-alcoholic fatty liver disease. J Hepatol 75: 150-162, 2021.
50. Ghrayeb A, Finney AC, Agranovich B, Peled D, Anand SK, McKinney MP, Sarji M, Yang D, Weissman N, Drucker S, *et al*: Serine synthesis via reversed SHMT2 activity drives glycine depletion and acetaminophen hepatotoxicity in MASLD. Cell Metab 36: 116-129.e7, 2024.
51. Chen S, Lu Z, Jia H, Yang B, Liu C, Yang Y, Zhang S, Wang Z, Yang L, Li S, *et al*: Hepatocyte-specific Mas activation enhances lipophagy and fatty acid oxidation to protect against acetaminophen-induced hepatotoxicity in mice. J Hepatol 78: 543-557, 2023.
52. Fontana RJ: Pathogenesis of idiosyncratic drug-induced liver injury and clinical perspectives. Gastroenterology 146: 914-928, 2014.
53. Chao X, Wang H, Jaeschke H and Ding WX: Role and mechanisms of autophagy in acetaminophen-induced liver injury. Liver Int 38: 1363-1374, 2018.
54. Suciu M, Gruia AT, Nica DV, Azghadi SM, Mic AA and Mic FA: Acetaminophen-induced liver injury: Implications for temporal homeostasis of lipid metabolism and eicosanoid signaling pathway. Chem Biol Interact 242: 335-344, 2015.
55. Yan M, Huo Y, Yin S and Hu H: Mechanisms of acetaminophen-induced liver injury and its implications for therapeutic interventions. Redox Biol 17: 274-283, 2018.
56. Hanawa N, Shinohara M, Saberi B, Gaarde WA, Han D and Kaplowitz N: Role of JNK translocation to mitochondria leading to inhibition of mitochondria bioenergetics in acetaminophen-induced liver injury. J Biol Chem 283: 13565-13577, 2008.
57. Huo Y, Yin S, Yan M, Win S, Aung Than T, Aghajan M, Hu H and Kaplowitz N: Protective role of p53 in acetaminophen hepatotoxicity. Free Radic Biol Med 106: 111-117, 2017.
58. Antoniades CG, Quaglia A, Taams LS, Mitry RR, Hussain M, Abeles R, Possamai LA, Bruce M, McPhail M, Starling C, *et al*: Source and characterization of hepatic macrophages in acetaminophen-induced acute liver failure in humans. Hepatology 56: 735-746, 2012.
59. Jaeschke H and Liu J: Neutrophil depletion protects against murine acetaminophen hepatotoxicity: Another perspective. Hepatology 45: 1588-1589, 2007.
60. Liu ZX, Han D, Gunawan B and Kaplowitz N: Neutrophil depletion protects against murine acetaminophen hepatotoxicity. Hepatology 43: 1220-1230, 2006.
61. Cover C, Liu J, Farhood A, Malle E, Waalkes MP, Bajt ML and Jaeschke H: Pathophysiological role of the acute inflammatory response during acetaminophen hepatotoxicity. Toxicol Appl Pharmacol 216: 98-107, 2006.
62. Yang W, Tao Y, Wu Y, Zhao X, Ye W, Zhao D, Fu L, Tian C, Yang J, He F and Tang L: Neutrophils promote the development of reparative macrophages mediated by ROS to orchestrate liver repair. Nat Commun 10: 1076, 2019.
63. Niu B, Lei X, Xu Q, Ju Y, Xu D, Mao L, Li J, Zheng Y, Sun N, Zhang X, *et al*: Protecting mitochondria via inhibiting VDAC1 oligomerization alleviates ferroptosis in acetaminophen-induced acute liver injury. Cell Biol Toxicol 38: 505-530, 2022.
64. Todorović Vukotić N, Đorđević J, Pejić S, Đorđević N and Pajović SB: Antidepressants- and antipsychotics-induced hepatotoxicity. Arch Toxicol 95: 767-789, 2021.
65. Cuenda A and Sanz-Ezquerro JJ: p38γ and p38δ: From spectators to key physiological players. Trends Biochem Sci 42: 431-442, 2017.
66. Gaestel M, Kotlyarov A and Kracht M: Targeting innate immunity protein kinase signalling in inflammation. Nat Rev Drug Discov 8: 480-499, 2009.
67. Escós A, Risco A, Alsina-Beauchamp D and Cuenda A: p38γ and p38δ mitogen activated protein kinases (MAPKs), new stars in the MAPK galaxy. Front Cell Dev Biol 4: 31, 2016.
68. Xu W, Liu R, Dai Y, Hong S, Dong H and Wang H: The role of p38γ in cancer: From review to outlook. Int J Biol Sci 17: 4036-4046, 2021.
69. Yin DP, Zheng YF, Sun P, Yao MY, Xie LX, Dou XW, Tian Y and Liu JS: The pro-tumorigenic activity of p38γ overexpression in nasopharyngeal carcinoma. Cell Death Dis 13: 210, 2022.
70. Meng F, Zhang H, Liu G, Kreike B, Chen W, Sethi S, Miller FR and Wu G: p38γ mitogen-activated protein kinase contributes to oncogenic properties maintenance and resistance to poly (ADP-ribose)-polymerase-1 inhibition in breast cancer. Neoplasia 13: 472-482, 2011.
71. González-Terán B, Matesanz N, Nikolic I, Verdugo MA, Sreeramkumar V, Hernández-Cosido L, Mora A, Crainiciuc G, Sáiz ML, Bernardo E, *et al*: p38γ and p38δ reprogram liver metabolism by modulating neutrophil infiltration. EMBO J 35: 536-552, 2016.
72. Zhu X, Zhao Z, Zhang Y, Li H, Zhou X, Zhu Y, Chen Q, Kan S, Zhou L and Zhao G: p38γ modulates ferroptosis in brain injury caused by ethanol and cerebral ischemia/reperfusion by regulating the p53/SLC7A11 signaling pathway. Cell Signal 131: 111728, 2025.
73. Sun YM, Lin KY and Chen YQ: Diverse functions of miR-125 family in different cell contexts. J Hematol Oncol 6: 6, 2013.
74. Wang C, Huang W, Lin J, Fang F, Wang X and Wang H: Triclosan-induced liver and brain injury in zebrafish (Danio rerio) via abnormal expression of miR-125 regulated by PKCα/Nrf2/p53 signaling pathways. Chemosphere 241: 125086, 2020.
75. Xie C, Zhang LZ, Chen ZL, Zhong WJ, Fang JH, Zhu Y, Xiao MH, Guo ZW, Zhao N, He X and Zhuang SM: A hMTR4-PDIA3P1-miR-125/124-TRAF6 regulatory axis and its function in NF kappa B signaling and chemoresistance. Hepatology 71: 1660-1677, 2020.
76. Zhang Z, Moon R, Thorne JL and Moore JB: NAFLD and vitamin D: Evidence for intersection of microRNA-regulated pathways. Nutr Res Rev 36: 120-139, 2023.
77. Fabian MR and Sonenberg N: The mechanics of miRNA-mediated gene silencing: A look under the hood of miRISC. Nat Struct Mol Biol 19: 586-593, 2012.
78. Gjorgjieva M, Sobolewski C, Dolicka D, Correia de Sousa M and Foti M: miRNAs and NAFLD: From pathophysiology to therapy. Gut 68: 2065-2079, 2019.
79. Wang H, Mehal W, Nagy LE and Rotman Y: Immunological mechanisms and therapeutic targets of fatty liver diseases. Cell Mol Immunol 18: 73-91, 2021.
80. Dong ZB, Wu HM, He YC, Huang ZT, Weng YH, Li H, Liang C, Yu WM and Chen W: MiRNA-124-3p.1 sensitizes hepatocellular carcinoma cells to sorafenib by regulating FOXO3a by targeting AKT2 and SIRT1. Cell Death Dis 13: 35, 2022.
81. Xu H, Tian Y, Tang D, Zou S, Liu G, Song J, Zhang G, Du X, Huang W, He B, *et al*: An endoplasmic reticulum stress-MicroRNA-26a feedback circuit in NAFLD. Hepatology 73: 1327-1345, 2021.
82. Hoxhaj G and Manning BD: The PI3K-AKT network at the interface of oncogenic signalling and cancer metabolism. Nat Rev Cancer 20: 74-88, 2020.
83. Ye Q, Liu Y, Zhang G, Deng H, Wang X, Tuo L, Chen C, Pan X, Wu K, Fan J, *et al*: Deficiency of gluconeogenic enzyme PCK1 promotes metabolic-associated fatty liver disease through PI3K/AKT/PDGF axis activation in male mice. Nat Commun 14: 1402, 2023.

84. Esposito A, Viale G and Curigliano G: Safety, tolerability, and management of toxic effects of phosphatidylinositol 3-kinase inhibitor treatment in patients with cancer: A review. JAMA Oncol 5: 1347-1354, 2019.
85. Funato Y, Michiue T, Asashima M and Miki H: The thioredoxin-related redox-regulating protein nucleoredoxin inhibits Wnt-beta-catenin signalling through dishevelled. Nat Cell Biol 8: 501-508, 2006.
86. Ren Y, Yang X, Niu X, Liu S and Ren G: Chemical characterization of the avenanthramide-rich extract from oat and its effect on D-galactose-induced oxidative stress in mice. J Agric Food Chem 59: 206-211, 2011.